REFRACTORY METAL TO NICKEL-BASED ALLOY JOINING TECHNOLOGIES

FOR HIGH TEMPERATURE APPLICATIONS

Except where reference is made to the work of others, the work described in this thesis is my own or was done in collaboration with my advisory committee. This thesis does not include proprietary or classified information.

_____

Chad M. Callender

Certificate of Approval:

_____	_____
Jeffrey W. Fergus Associate Professor Materials Engineering	William F. Gale, Chair Professor Materials Engineering
_____	_____
Lewis Payton Assistant Research Professor Industrial and Systems Engineering	Stephen L. McFarland Dean Graduate School

REFRACTORY METAL TO NICKEL-BASED ALLOY JOINING TECHNOLOGIES FOR HIGH TEMPERATURE APPLICATIONS

Chad M. Callender

A Thesis

Submitted To

The Graduate Faculty of

Auburn University

In Partial Fulfillment of the

Requirements for the

Degree of

Master of Science

Auburn, Alabama
August 7, 2006

REFRACTORY METAL TO NICKEL-BASED ALLOY JOINING TECHNOLOGIES FOR HIGH TEMPERATURE APPLICATIONS

Chad M. Callender

Permission is granted to Auburn University to make copies of this thesis at its discretion, upon the request of individuals or institutions and at their expense. The author reserves all publication rights.

_____
Signature of Author

_____
Date of Graduation

VITA

Chad M. Callender, son of Charles R. and Lora S. Callender, was born on October 20, 1975 in San Antonio, Texas. After graduating from Pemberton Township High School, New Jersey in 1993 he joined the United States Navy and remained on active duty throughout his academic career. He married Stephanie D. McDaniel, daughter of Jerry and Nancy McDaniel of Hendersonville, North Carolina on May 30, 1998. He attended Auburn University, Alabama where he graduated Summa Cum Laude with a Bachelor of Materials Engineering degree in August 2004. He then entered graduate school at Auburn University in August of 2004 as a graduate research and teaching assistant.

REFRACTORY METAL TO NICKEL-BASED ALLOY JOINING TECHNOLOGIES FOR HIGH TEMPERATURE APPLICATIONS

Chad M. Callender

Master of Science, August 7, 2006
(B.S., Auburn University, 2004)

96 Typed Pages

Directed by William F. Gale

This thesis provides a detailed description of efforts towards the joining of niobium (Nb) to nickel-based alloys in order to increase the overall efficiency of gas turbine-based power generation systems. The desired increase in efficiency can be achieved by allowing for higher operating temperatures. In addition to the thermal efficiency of the power generating systems, their long-term reliability is also a major concern.

Nickel-based superalloys were developed for the sole purpose of satisfying requirements for high-temperature component materials. Some factors which contribute to the selection of nickel-based superalloys for use in these systems are their inherent high modulus of elasticity, excellent hot corrosion resistance, high creep resistance and superior strength at high temperatures. Refractory metals, or metals that have melting

points that exceed 2450°C and their alloys also make excellent candidates for potential structural materials for high efficiency power generation systems due to their high melting temperatures and their good physical properties such as low thermal expansion coefficients, high thermal conductivities, and high Young's moduli. Because both the strength and ductility of refractory metals are greatly affected by adverse microstructural changes that occur when their respective recrystallization temperatures are exceeded, conventional welding techniques are strength prohibitive for use in joining these metals. Therefore, joining these metals is best accomplished by a form of high temperature brazing known as transient liquid phase (TLP) bonding.

With superalloys and refractory metals being strong potential candidates for high temperature and high efficiency power generation systems, a suitable technique is needed to produce an effective joint between these materials while retaining their base physical properties. Careful consideration must be used when designing the overall joint to avoid the formation of potentially harmful intermetallic phases. This can be accomplished by inserting diffusion barriers where needed. The final result is a joint that requires several substrate materials and successive TLP bonds to complete.

The joint design, developed in this project, employs the use of several TLP bonds between a series of spacer interlayers linking pure nickel and niobium substrates. This design is used to prevent the substrates, Ni and Nb, from contacting to prevent formation of the intermetallic phases mentioned before. All of the TLP bonds are successful in terms of initial microstructure/microhardness and room-temperature mechanical testing.

ACKNOWLEDGMENTS

I would like to thank Dr. William F. Gale for his support and guidance throughout my graduate career. The character and engineering traits that Dr. Gale has taught me will be invaluable for the remainder of my career. I would also like to thank Dr. Lewis Payton, Dr. Jeff Fergus, Dr. Tony Overfelt, and Dave Lindahl for their help, advice, guidance, and encouragement during my stay at Auburn University.

In addition, I would like to thank the United States Navy for affording me the opportunity to earn my graduate degree while serving on active duty. I would also like to thank my friends and colleagues at Auburn University who have made the experiences here memorable ones, and Robert Love, Andrew Gay, and Venu Krishnardula for their technical assistance during the experimentation phase of this thesis project.

I would especially like to thank my wife, Stephanie, and my son, Hutson for their undying support and understanding during my studies. My success is a direct reflection of their acceptance and consideration for the importance of my work. Also, I would like to thank my parents for giving me strength and teaching me the character, work ethic, and morals that has made my education a success.

Style manual or journal used Metallurgical Transactions A

Computer software used Microsoft Word 2003

TABLE OF CONTENTS

LIST OF TABLES XI

LIST OF FIGURES XII

1. INTRODUCTION 1

2. LITERATURE REVIEW 5

2.1 Current and Future Need for High Temperature Materials 5
2.2 Possible Materials to be Used in High Temperature Applications 9
2.2.1 Superalloys 9
2.2.2 Intermetallics 14
2.2.3 Ceramics 17
2.2.4 Composites 18
2.2.5 Refractory Metals 22
2.2.6 Material Selection 24
2.3 The Need for Joining and Joining Methods 24
2.3.1 Diffusion Bonding 28
2.3.2 Brazing 29
2.3.3 Transient Liquid Phase (TLP) Bonding 29

3. RESEARCH OBJECTIVES 32

4. JOINT MATERIALS AND EXPERIMENTAL PROCEDURES 35

4.1 Possible Joint Combinations 35
4.2 Bonding Specimen Preparation 43
4.3 Diffusion Bond Design and Attempts 43
4.4 Joint Design Incorporating TLP Bonding 45
4.5 Metallographic Sample Preparation 50
4.6 Specimen Characterization 50
4.7 Mechanical Testing 51
4.7.1 Hardness Testing 51
4.7.2 Shear Testing 51

5. RESULTS AND DISCUSSION 54

5.1 Characterization of Individual Bonds 54
5.1.1 Nb-Mo TLP Bond 54
5.1.2 Ni-Pd TLP Bonds 56
5.1.3 Mo-Pd TLP Bond 59
5.2 Mechanical Testing of Individual Bonds 61
5.2.1 Micro-Hardness Testing 61
5.2.2 Shear Testing 64
5.3 Modeling 67
5.3.1 The Ni-Ti-Mo TLP Bond 68
5.3.2 The Pd-BNi6-Ni TLP Bond 71
5.3.3 The Pd-BNi3-Ni TLP Bond 72
5.3.4 The Mo-Pd/Cu-Pd TLP Bond 72

6. SUMMARY AND CONCLUSIONS 75

7. RECOMMENDATIONS FOR FUTURE WORK 77

8. REFERENCES 79

LIST OF TABLES

Table 1 - Physical properties of two intermetallics with higher melting temperatures compared to a Ni-based superalloy [1] 16

Table 2 - Strength and toughness of some CMC's compared with those of the corresponding monolithic ceramics [1] 19

Table 3 - Physical properties of four refractory metals compared to a Ni-based superalloy [1] 23

Table 4 - Summary of comparisons made for each type of material studied for potential use in high temperature applications..... 26

Table 5 - Comparison of all available couple combinations with Ni 36

Table 6 - Comparison of all available couple combinations with Nb 37

Table 7 - Comparison of all available couple combinations with Pd..... 38

Table 8 - Comparison of all available couple combinations with Pt..... 39

Table 9 - Comparison of all available couple combinations with Mo 40

Table 10 - Nominal compositions and melting temperatures of BNi-3 and BNi-6 [50]..... 48

Table 11 - Shear test data for each TLP bond used in the overall joint design..... 65

LIST OF FIGURES

Figure 1 - Past trends of atmospheric concentrations of CO_2 along with anthropogenic emissions [12] 6

Figure 2 - Relationship between thermal efficiencies of power plant to corresponding turbine inlet temperatures [1] 8

Figure 3 - Creep-rupture strengths of superalloys [16] 13

Figure 4 - Force versus displacement graph of a monolithic ceramic, a fiber-reinforced (or CMC) ceramic, and a particulate-reinforced ceramic [29] 20

Figure 5 - Comparison of specific strengths versus temperature of various alloys [1] 27

Figure 6 - Stages in a TLP bonding process using a substrate with composition A (C_A) and an interlayer with eutectic composition (C_E). (a) Initial condition; (b) Dissolution of interlayer; (c) Isothermal solidification; (d) Completion of isothermal solidification; (e) Solid state homogenization; (f) Final condition; C_L = liquidus composition; C_S = solidus composition; T_B = bonding temperature [37] 31

Figure 7 - Ni-Nb equilibrium binary phase diagram [49] 33

Figure 8 - Mo-Pd equilibrium binary phase diagram [49] 42

Figure 9 - Schematic of the two diffusion couples attempted 44

Figure 10 - Schematic of the current bonding sequence using three distinct TLP bonds to create the overall Ni to Nb joint 46

Figure 11 - Cu-Pd equilibrium binary phase diagram with the TLP interlayer nominal composition annotated for the Mo-Pd bond [49] 49

Figure 12 - Diagram of shear test specimen dimensions used for each TLP bond ... 52

Figure 13 - Photographs of the shear testing device used on each TLP bond [52] ... 53

Figure 14 - Micrograph of Nb-Mo TLP bond using a 12.5µm Ti interlayer 55

Figure 15 - Micrograph of Ni-Pd TLP bond using a 25µm BNi-6 interlayer. The large dark areas in the Ni region of the bond are due to damage incurred during polishing. These might have contained phosphides, which have fallen out during polishing, although marked comet-tails were not apparent..... 57

Figure 16 - Micrograph of Ni-Pd TLP bond using a 25µm BNi-3 interlayer. The large dark areas in the Pd region of the bond are due to damage incurred during polishing. These might have contained borides, which have fallen out during polishing, although marked comet-tails were not apparent..... 58

Figure 17 - Micrograph of Mo-Pd TLP bond using a 0.08mm Pd-Cu interlayer. The large dark areas in the Mo region of the bond are most likely borides that fell out during polishing..... 60

Figure 18 - Graph of microhardness values taken from all TLP bonds created..... 62

Figure 19 - Graph of relative microhardness values taken from all TLP bonds created..... 63

Figure 20 - Photograph of Mo-Pd bond following shear testing. The upper portion if the Pd while the lower is Mo..... 66

Figure 21 - Three different solute concentration lines in the bond substrates at three different times and also a theoretical solubility limit for α-Ti in both substrates [59]..... 70

1. INTRODUCTION

Due to recent rises in global environmental concerns and long-term increases in the cost of crude oil and natural gas, there has been a significant thrust for higher efficiency power generation systems [1]. The desired increase in efficiency can be achieved by allowing for higher operating temperatures of gas turbine-based power generation systems [1-3]. In addition to the thermal efficiency of the power generating systems, the long-term reliability is also a major concern. There is a strong current demand for materials that can meet these requirements with foremost attention being placed on the materials' ability to resist creep, oxidation, hot corrosion, and thermal fatigue [1].

Nickel-based superalloys were developed for the sole purpose of satisfying these requirements. Some factors which contribute to these properties are the inherent high modulus of elasticity of superalloys and the use of alloying elements such as titanium and aluminum that allow for the formation of γ' phases, or phases formed by the addition of certain elements to the alloy such as Al and Ti. These γ' phases, if dispersed homogeneously throughout the microstructure, have a hardening effect. The addition of chromium aids in hot corrosion resistance at the price of reduction in the γ' content while carbon content, in some superalloys, is maintained high enough to allow for the formation of carbides. The carbides produced in the superalloy improve its' resistance to

creep [1,4]. Also, solid solution C is needed in polycrystalline superalloys for grain boundary strengthening [1].

Refractory metals, or metals that have melting points that exceed 2450°C [5], and their alloys also make excellent candidates for potential structural materials for high efficiency power generation systems due to their high melting temperatures and their good physical properties such as thermal expansion coefficients, thermal conductivities, and Young's moduli [1,5]. Some examples of refractory metals include niobium (Nb), molybdenum (Mo), tantalum (Ta), rhenium (Re), and tungsten (W). While all of these metals exhibit strong characteristics for being potential candidates for use in power generation components, most refractory metals are adversely affected by a high ductile-to-brittle transition temperature (DBTT) such as molybdenum (Mo), which is brittle at room temperature. However niobium (Nb), because of its low temperature ductility and moderate density, is the most attractive choice for a refractory metal in this system [1]. While the base properties of some refractory metals are sufficient for structural applications, a suitable joining technique is needed to satisfy the requirements set forth in any system design such as high operating temperatures and extended operation times. Also, it is important to point out that, for oxidizing atmospheres, use of refractory metals other than rhenium (Re) is limited by oxidation and oxygen embrittlement [5].

Because both the strength and ductility of refractory metals are greatly affected by adverse microstructural changes that occur when their respective recrystallization temperatures are exceeded, conventional welding techniques are strength prohibitive for use in joining these metals [5-7]. Therefore, joining refractory metals is best accomplished by a form of high temperature brazing known as transient liquid phase

(TLP) bonding. In a conventional brazing process, a filler metal is chosen based on its melting temperature being significantly below the melting temperature of the substrate materials [8]. However, the overall strength and maximum operating temperature of the final joint is severely limited because the filler metal is still present in the joint [9].

Similar to brazing, TLP bonding can be performed at a temperature significantly lower than the substrate melting temperatures, and indeed the recrystallization temperatures, of the substrate metals depending on the choice of the filler metal. Bonding temperature will depend on the melting temperature of the filler metal and therefore the metal can be chosen based on its solubility with the substrate and its own melting point. In TLP bonding, the liquid filler metal re-solidifies at the bonding temperature due to compositional changes resulting from interdiffusion with the substrate materials. This process potentially results in a joint that has similar microstructural characteristics, and hence mechanical properties to that of the parent substrate material [9].

Nickel-based superalloys have a typical operating range of 1000°C to 1100°C [1]. For any application where a higher operating temperature is necessary, a refractory metal or alloy is required. With superalloys and refractory metals being strong potential candidates for high temperature and high efficiency power generation systems, a suitable technique is needed to produce an effective joint between these materials while retaining their base physical properties. Careful consideration must be used when designing the overall joint to avoid the formation of potentially harmful intermetallic phases. This avoidance of harmful intermetallic phases can be accomplished by inserting diffusion

barriers where needed. The final result is a joint that requires several substrate materials and successive TLP bonds to complete.

2. LITERATURE REVIEW

2.1 Current and Future Need for High Temperature Materials

Increasing global environmental and fuel supply issues have created an escalating demand for higher efficiencies in power generation systems [1]. Current and future systems will be forced to meet increasing demands for extended periods of time requiring less fuel consumption and exhausting less environmentally harmful pollutants into the atmosphere [10,11].

To understand why it is necessary to reduce the amount of pollutants exhausted, we must first recognize what these pollutants do to the atmosphere and the environment. Chemical compounds such as CO, CO_2, SO_2, and NO_x act as greenhouse gases. Greenhouse gases are defined by the Energy Information Administration (EIA), a division of the Department of Energy (DOE), as gases that allow sunlight to enter the earth's atmosphere freely and then are heated by absorbing infrared radiation. This heat is then trapped in the atmosphere causing global warming to occur [12]. Carbon dioxide (CO_2) is thought to be the greenhouse gas that is the most significant contributor to global warming [12,13]. Atmospheric CO_2 levels have been rising rapidly over the past one hundred years as seen in Figure 1.

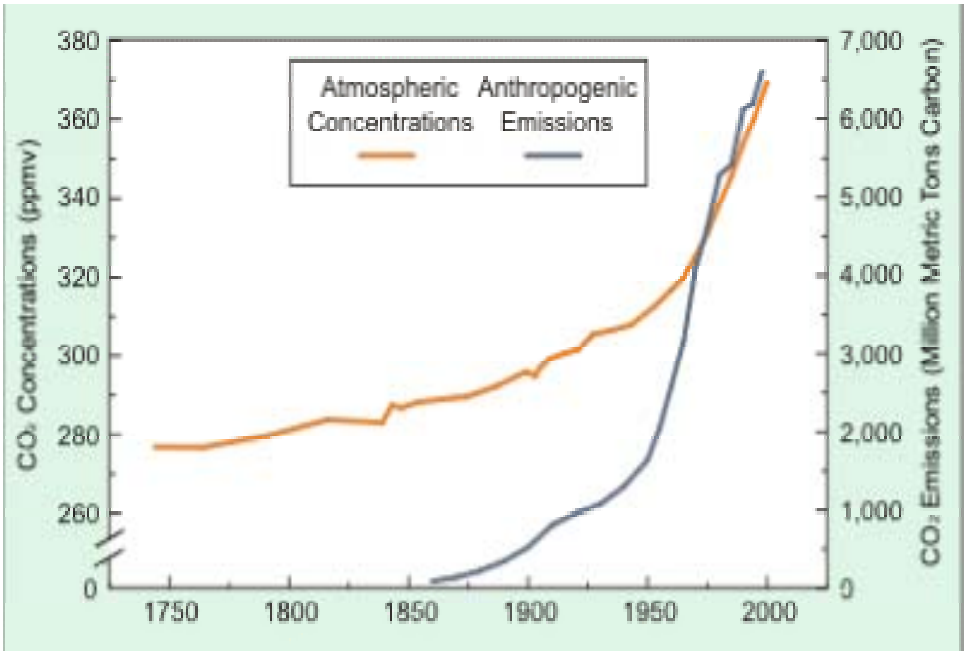

Figure 1. Past trends of atmospheric concentrations of CO_2 along with the anthropogenic emissions [12]. Anthropogenic emissions are those that are considered man-made.

In addition to the concerns about environmental pollutants released and their potential effects on global warming, the limited supply of fuel for these power generation systems also produces a need for increased operating efficiencies. It is now well understood that there is a very limited amount of petroleum products that exist in the world given the fact that oil is a non-renewable source [14].

Therefore, from an environmental point of view, increasing the thermal efficiencies and performance of power generation systems is an excellent method to conserve precious energy and diminish the environmental impacts as a result of producing power [14].

Increased efficiencies can be accomplished by increasing the operating temperatures or turbine inlet temperatures (TIT) of turbine-based power generation cycles [1,2,3]. This effect is shown in Figure 2 [1]. As a result of the demands for higher thermal efficiencies, there is a growing demand for materials that can maintain long term reliability and resist high temperature creep, thermal shock, oxidation, and corrosion at these elevated temperatures [1].

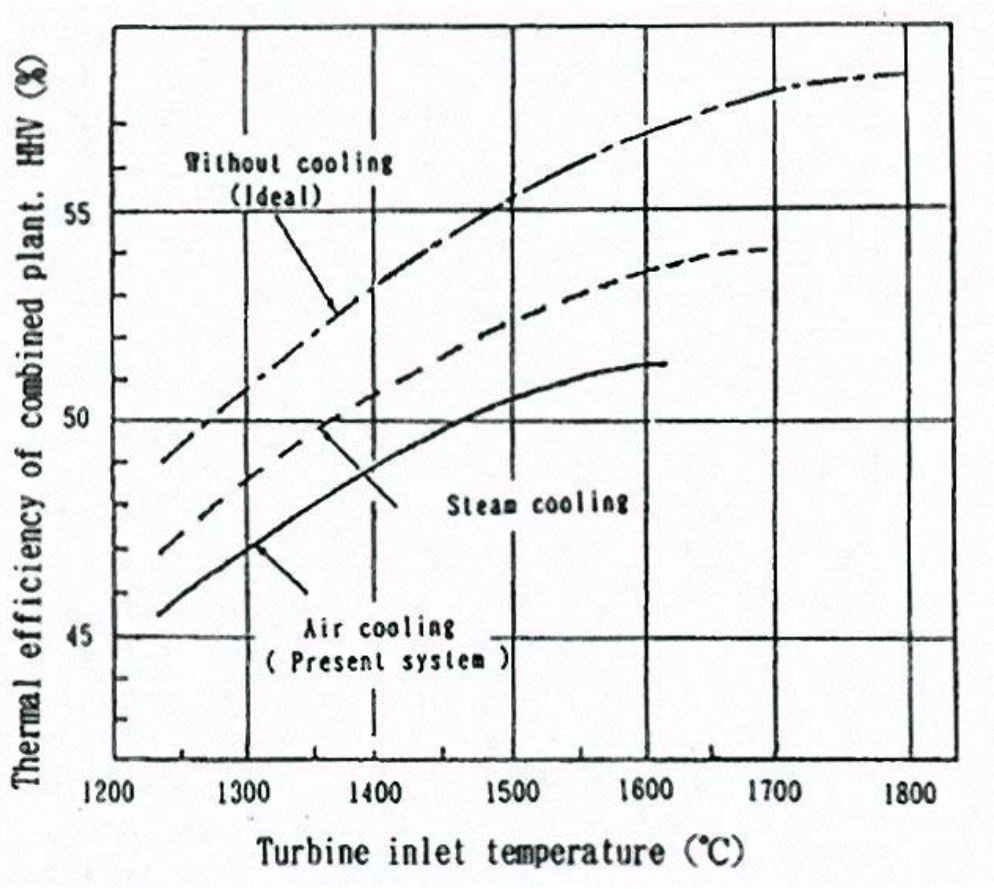

Figure 2. Relationship between thermal efficiencies of power plant to corresponding turbine inlet temperatures [1].

2.2 Possible Materials to be Used in High Temperature Applications

As indicated in Section 2.1, there has been a significant amount of research over the last 60 or so years in the field of high temperature materials. While some of the materials most commonly associated with high temperature applications, such as most ceramics, are not suitable for power generation systems due to their brittleness, there are numerous alternatives including superalloys, refractory metals, intermetallics, and composite materials such as ceramic matrix composites (CMC's) and metal matrix composites (MMC's). A brief discussion of ceramic materials will be included in this section as there is ongoing research and development toward being able to use these materials or enhance their application for superalloys in turbine-based power generation equipment.

2.2.1 Superalloys

Currently, there are three main categories of superalloys that include iron (iron nickel)-based, nickel-based, and cobalt-based alloys [1,15]. They were all designed to offer strong, corrosion-resistant materials for high-temperature applications and have the ability to maintain these characteristics, even after long exposure times to elevated temperatures [15,16]. The resourcefulness of these alloys is derived from their ability to combine their high strengths and allowable operating temperatures with good low-temperature ductility and excellent surface stability [15].

Most metal's strengths are best considered in terms of their short-term properties such as yield strength and ultimate tensile strength, given their use at moderate

temperatures. In contrast, a superalloy's strength is better considered at higher temperatures of approximately 50% or higher of the absolute melting point or range [16], given that these materials are intended for prolonged high temperature service. Therefore, stress-rupture (creep-rupture) tests are often performed on superalloys to determine their overall strength and their potential applications. Figure 3 is a graph of the results of creep-rupture tests performed on all three types of superalloys. Steady-state creep rate is also very important for engineering applications.

From Figure 3, it can be concluded that the iron nickel and nickel-based superalloys have the highest stress-rupture strengths when compared to carbide-phase-strengthened cobalt alloys and solid-solution-strengthened iron, nickel, and cobalt alloys. These characteristics are due to several inherent factors of these superalloys including [15-19]:

- γ Matrix- a continuous FCC nickel-based phase that contains a high percentage of solid-solution elements such as Co, Fe, Cr, Mo, and W.
- γ' Phases- formed from Al and Ti with a nominal composition of $Ni_3(Al,Ti)$. They react with the Ni to precipitate a phase that is coherent with the austenitic γ matrix. Both the γ' phase and the matrix are cubic (the matrix is FCC while γ' is primitive cubic) but have different lattice parameters. This lattice mismatch creates coherency strains, depending on the degree of misfit, and inhibits dislocation migration. Appears as spheres or cuboids with a bimodal distribution and is the principal high temperature strengthening phase.

- γ' Films- produced by heat treatments and service temperature exposure. They form along the grain boundaries and therefore may be beneficial to creep-rupture properties.
- γ' Rafts- elongated γ' in the grains. Results from γ' being placed under stress. May or may not be useful for increasing creep-rupture strengths. Depends on γ/ γ' misfit.
- γ'' Phases- Ni and Nb combine in the presence of Fe to form a BCT phase that is coherent with the γ matrix with a nominal composition of Ni_3Nb. This phase induces large mismatch strains and provides for high strengths at low to mid temperatures. However, it is unstable at high temperatures and can form a δ phase (orthorhombic Ni_3Nb intermetallic compound). This phase in incoherent and does not confer strength when it is present in large quantities. Therefore, joining γ'' formers is difficult without the use of heat treatments to eliminate detrimental intermetallics.
- Carbides- carbon combines with elements such as Ti, Ta, Hf, and Nb to form metal carbides such as MC, $M_{23}C_6$, M_6C, and M_7C_3 (less common than others). Directly, carbides may provide limited strengthening (through dispersion hardening). However, and more commonly in polycrystalline substrates, C provides indirect strengthening by stabilizing grain boundaries against excessive shear as long as the C content is below the solubility limit. Therefore, C is not typically added to single crystal alloys.

- Borides- Boron (B) and other elements such as Zr and Hf are added to enhance mechanical and chemical properties of polycrystalline alloys. B acts much the same way as C in that it provides some amount of indirect strengthening in the grain boundaries provided it is below the solubility limit. Also, boride particles may form as boron segregates to the grain boundaries. Several boride phases also exist. Small amounts of boride phases are good for creep-rupture properties.
- Topologically Close-Packed (TCP) Phases- The atoms in this phase are stacked in the sequence ABCABC however, they are in-fact not close-packed in all three dimensions which results in an inherent brittleness. They appear as plate or needle-like phases that may form under certain conditions with compositions such as Co_2W_6 (μ phase), Fe_2Nb (Laves), and FeCr (σ phase). These phases cause lowered creep-rupture strengths and ductility.

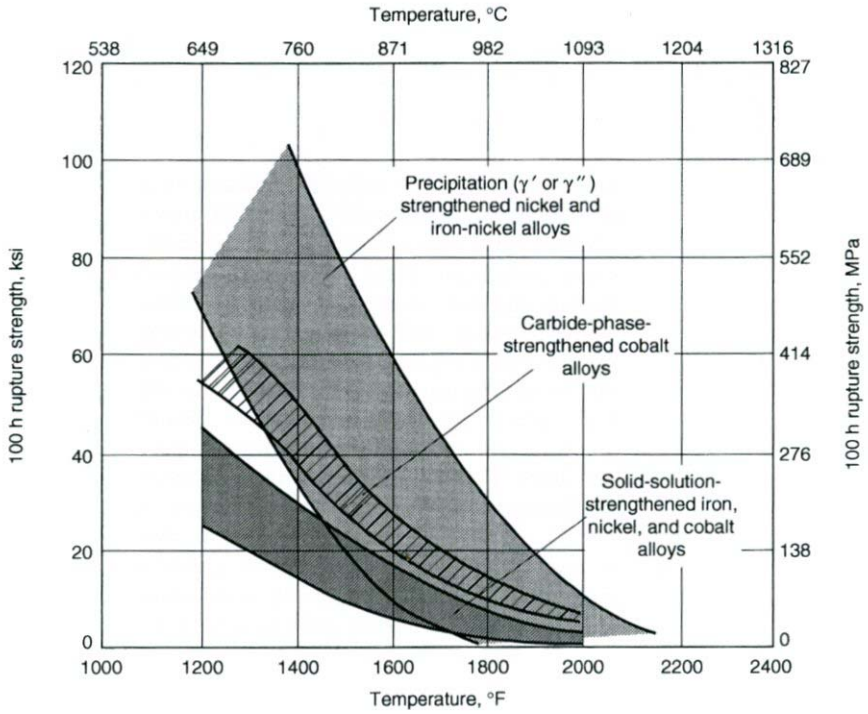

Figure 3. Creep-rupture strengths of superalloys [16].

2.2.2 Intermetallics

Another candidate material for high temperature applications is structural intermetallics, or alloys comprised of two or more metals having a characteristic ordered crystal structure and a definite composition. Typically, intermetallics are recognized for having a high specific modulus, superb strength, low density (depending on composition), and excellent oxidation and corrosion resistance [1,20,21].

Ordered intermetallics based on the aluminides of transition metals such as Ni, Fe, Ti, Nb, and Co have been studied in great detail recently. While they exhibit high heat resistances up to temperatures of around 1100°C, their room temperature ductility and fracture toughness is very poor making them difficult to process and fabricate into usable parts and also vulnerable during installation and service [1,20]. Due to this problem, much of the recent work has been spent in developing intermetallics with improved room temperature ductility and toughness to raise their potential for use in practical applications [1].

Most recently, research has been dedicated in the areas of alloy composition, derivation from stoichiometry, and ternary alloying additions to create multiphase intermetallic alloys that contain controlled microstructures such as γ-TiAl and its alloys and the B2 intermetallic alloys such as NiAl [1]. While the room temperature ductility has been improved to over 20% in a three-phase alloy consisting of Co, Ni, Ti, and Al, the high temperature strengths of these alloys remain lower than that of superalloys [1,22].

While the temperature capabilities of Ti-Al systems are limited to around 760°C from the standpoint of high-temperature creep and oxidation resistance, efforts have also been focused on intermetallic alloys with higher melting temperatures such as $MoSi_2$ and Nb_3Al [1,23,24]. Their physical properties are indexed in Table 1 [1] along with the physical properties of a typical Ni-based superalloy MarM-246. The $MoSi_2$ exhibits excellent oxidation resistance while the Nb_3Al does not and they both are very brittle at room temperature [1]. A solution has yet to be found for enough low temperature ductility coupled with sufficient oxidation resistance.

Table 1. Physical properties of two intermetallics with higher melting temperatures compared to a Ni-based superalloy [1].			
	Intermetallic Alloys		Ni-Based Superalloy
Physical Properties	Nb_3Al	$MoSi_2$	MarM-246
Density (kg/m^3)	7300	6200	8440
Melting Temperature (°C)	1960	2020	1315
Thermal Expansion Coefficient (10^{-6} K^{-1})	9.15	8.25	11.3
Thermal Conductivity ($W*m^{-1}K$)	12.6	48.6	15
Young's Modulus (GPa)	-	440	200

2.2.3 Ceramics

Monolithic engineering ceramics are known for their high temperature capability, moderate creep strength, good wear resistance, and high thermal conductivity [1,25-27]. A high thermal conductivity is important because it indicates a materials ability to evenly distribute heat throughout its entire area. Having a high thermal conductivity means that the temperature gradients are small and therefore the material is less likely to undergo thermal shock. Therefore, the result of using a material with a high thermal conductivity is that internal blade cooling is more effective at reducing the temperature of the surface of the blade (i.e. hottest region of the blade). However, monolithic engineering ceramics are deficient in the area of fracture toughness when considering them for use in a modern power generation system [1,25]. SiC and Si_3N_4 are two of the more popular choices of monolithic ceramics due to their overall good mechanical properties but still contain the fatal flaw of being exceptionally brittle [1,26]. In addition to this problem, they are also relatively expensive to manufacture [1].

Oxide ceramics, such as Al_2O_3, have a higher resistance to oxidation at high temperatures than non-oxide ceramics such as SiC and Si_3N_4 [1]. Besides this inherent resistance to oxidation, oxide ceramics in single crystal form are inherently strong and have high melting points, high elastic moduli, and very low densities [27]. The limitation of polycrystalline oxide ceramics has typically been that they display easy plastic deformation above temperatures of 1000°C [1,27].

The most modern work with high temperature ceramics is in the field of ceramic-matrix composites [1].

2.2.4 Composites

An approach that has been used to alleviate the problem of low fracture toughness of monolithic ceramics is to incorporate long ceramic fibers into the matrix of the monolithic ceramic creating a ceramic-matrix composite (CMC) or continuous fiber ceramic composite (CFCC) [1,27-29]. Instead of increasing the tensile strength of the base material, the fibers actually improve the material's toughness and overall reliability by inhibiting crack propagation due the crack having to deflect, or change its direction, around the fiber reinforcement [1,29]. Table 2 [1] shows some examples of the results of fiber reinforcement on monolithic ceramics. The fracture behavior of these materials is strongly influenced by the fiber/matrix interface. Weak bonding at this interface allows for the crack to propagate around the fiber reinforcement rather than propagating directly through the fiber that would occur if the bonding were strong [25-27]. Figure 4 [29] is a force versus displacement graph of a monolithic ceramic, a fiber-reinforced (or CMC) ceramic, and a particulate-reinforced ceramic where small particles, instead of long fibers, are dispersed throughout the ceramic matrix. In this figure, it is quite noticeable that the area under the fiber-reinforced curve is much larger than either of the other two curves, which is a direct indication of higher fracture toughness.

Table 2. Strength and toughness of some CMC's compared with those of the corresponding monolithic ceramics [1].		
CMC/ Ceramics	**Flexural Strength (MPa)**	**Fracture Toughness (MPa*m$^{1/2}$)**
SiC/ LAS	830	17
LAS	200	2
SiCw/Al2O3	800	8.7
Al2O3	550	4~5
SiC/SiC	193	30
SiC	402	3.4

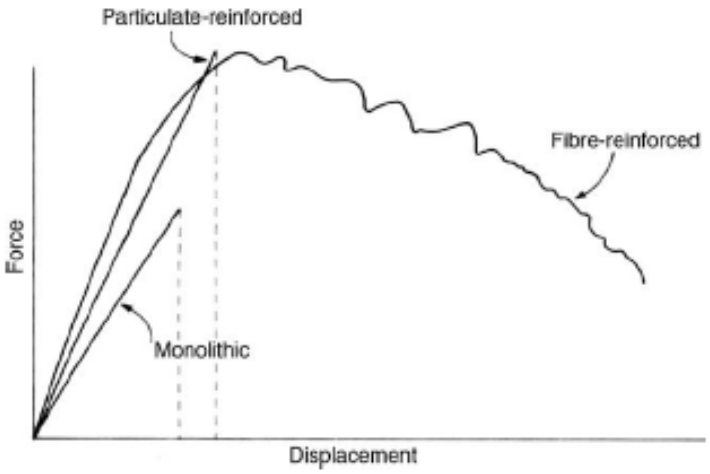

Figure 4. Force versus displacement graph of a monolithic ceramic, a fiber-reinforced (or CMC) ceramic, and a particulate-reinforced ceramic [29].

Metal matrix composites (MMC) are another form of composite material that have the capabilities required to be used in high temperature power generation systems. They are known for having a higher specific modulus, higher specific strength, better high temperature properties such as corrosion and creep resistance, lower coefficient of thermal expansion, and better wear resistance than their monolithic metal counterparts [29-32].

In general, MMC's consist of a metal matrix, typically an alloy [29], and some sort of reinforcement. These reinforcements are typically divided into five categories including: continuous fibers, discontinuous fibers, whiskers, wires, and particulates (including platelets) [23,29]. While the wire reinforcements are metallic, the rest of the reinforcements are generally ceramics including: oxides, carbides, and nitrides because of their excellent specific properties such as strength and stiffness and their high temperature properties [23,29-31].

While the attributes of MMC's were mentioned above, some of the cons of MMC's are [23]:

- They are costly to manufacture and use.
- The matrix and reinforcement are not in thermodynamic equilibrium. Therefore, a reaction can occur at high temperatures between them causing degradation of the fibers and reduce strength and fatigue resistance.

Both CMC's and MMC's appear to offer many of the desired properties for use in high temperature, high efficiency power generation systems but are still behind in overall fracture toughness when compared to that of superalloys. In addition to the lack of toughness exhibited by them, especially the CMC's (although these are better than the monolithic ceramics), they are both still extremely expensive to manufacture [1,29].

2.2.5 Refractory Metals

Refractory metals are metals that have melting points that exceed 2450°C [5]. These metals and their alloys also make excellent candidates for potential structural materials for high efficiency power generation systems due to their high melting temperatures and their good physical properties although the oxidation resistance is poor for most refractory metals [1,5]. These properties can be seen in Table 3 [1,33] and are compared to a typical Ni-based superalloy.

Nb has a moderate density of 8600 kg/m^3 and is comparable to that of the Ni-based superalloy MarM-246 with a density of 8440 kg/m^3. Mo, on the other hand, has a relatively large density of 10,200 kg/m^3 and suffers from a lack of low-temperature ductility while Nb has sufficient low-temperature ductility to be used for structural materials in power generation systems [1,34-36]. Also, Nb-based alloys have relatively high specific strengths and are comparable to those of Ni-based alloys between 1000°C and 1200°C as seen in Figure 5 [1]. These factors make Nb and its alloys excellent candidates for use in future high efficiency power generation systems with the exception that many of these involve oxidizing environments.

Table 3. Physical properties of three refractory metals compared to a Ni-based superalloy [1]. *Note: Based on 10h creep rupture test at designated stress with the exception of MarM-246 which is based on 1000h creep rupture test [33]. Quoted temperatures are in a vacuum.				
	Refractory Metals			Ni-Based Superalloy
Physical Properties	Nb	Ta	Mo	MarM-246
Density (kg/m^{-3})	8600	16600	10200	8440
Melting Temperature (°C)	2468	2996	2617	1315
Thermal Expansion Coefficient (10^{-6} K^{-1})	8.3	6.7	5.8	11.3
Thermal Conductivity (Ratio to MarM-246)	6.4	4.2	13.6	1
Young's Modulus (GPa)	110	186	289	200
Ductile to Brittle Transition Temperature (DBTT) (°C)	140	270	30	-
Maximum Use Temperature* (°C)	1095 at 37 MPa	1315 at 7 MPa	980 at 175 MPa	980 at 150 MPa

2.2.6 Material Selection

Table 4 provides a summary of the advantages and disadvantages of each classification of material reviewed for this project. Given the requirements of high temperatures and long operational lifetimes for the design of high efficiency power generation systems, the materials with the best mechanical properties to suit the job are superalloys up to their γ' solvus temperatures and Nb and its alloys above these temperatures. Currently, there have been exhaustive amounts of research in the field of Ni-based superalloys and their high temperature properties are well known and understood [1,4,15-18]. From Figure 5 [1], it is obvious that Nb and its alloys have higher maximum operating temperatures than Ni alloys and also have similar high temperature characteristics to Ni alloys. Therefore, Nb and its alloys would make ideal candidates for this application.

2.3 The Need for Joining and Joining Methods

With the understanding that there are several choices of materials that are capable of operating in the desired temperature range for an extended period of time, a suitable joining technique must be discovered that will also allow for the operational environments of the high efficiency power generation system. Due to the fact that the system will be composed of dissimilar materials, conventional joining techniques such electron beam (EB) welding and gas-tungsten arc (GTA) welding will not be suitable techniques because of the rapid heating and cooling effects produced from the welding [37]. These rapid heating and cooling processes cause many substrate materials to crack easily in air atmospheres [38]. Also, γ'-forming superalloys that do not characteristically

form γ'' are not typically weldable due to hot and post-weld heat treatment (PWHT) cracking [33]. This cracking is due to the combination of stresses, precipitation strengthening, and volumetric contraction that is associated with the formation of γ', which are results of the PWHT and strain-aging temperatures being the same. These temperatures also may be in the same range for γ'' however, γ'' precipitates at a much slower rate than γ' thus allowing the alloys to be heated into the solution temperature range without suffering aging and the resultant strain-age cracking [33]. Instead, alternative methods of joining such as diffusion bonding, brazing, and transient liquid phase (TLP) bonding must be explored.

Table 4. Summary of comparisons made for each type of material studied for potential use in high temperature applications.

Material Comparisons		
Class of Material	Pros	Cons
Ni-based Superalloys	▪ Well established and studied high temperature properties ▪ Excellent creep resistance	▪ 1000ºC-1100ºC maximum operating temperature band
Structural Intermetallics	▪ High specific modulus ▪ High strength ▪ Low density ▪ Excellent oxidation and corrosion resistance	▪ Low room temperature ductility ▪ Low fracture toughness
Monolithic Engineering Ceramics	▪ Moderate creep strength ▪ Good wear resistance ▪ High thermal conductivity compared to other ceramics	▪ Low fracture toughness ▪ Still a lower thermal conductivity than most metals
Composites (CMCs and MMCs)	▪ High specific modulus ▪ High specific strength ▪ Good corrosion and creep resistance at high temperatures ▪ Low coefficient of thermal expansion ▪ Good wear resistance	▪ Still costly to manufacture ▪ Matrix and reinforcement are not in thermodynamic equilibrium. (ex. TiSiC) ▪ Lack of toughness when compared to other materials.
Refractory Metals	▪ High melting temperatures ▪ High specific strengths (comparable to superalloys)	▪ Poor oxidation resistance at high temperatures (except Re) ▪ High densities

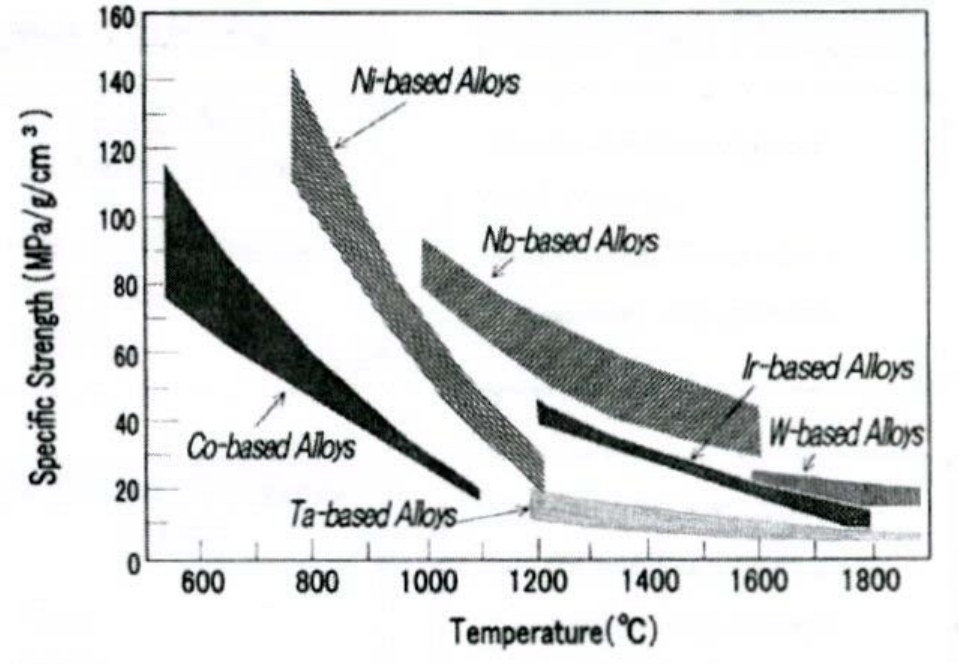

Figure 5. Comparison of specific strengths versus temperature of various alloys [1].

2.3.1 Diffusion Bonding

Diffusion bonding occurs isothermally while the two substrates remain in their solid-state form [37]. This process allows for the negation of the rapid heating and cooling as seen in conventional fusion welding techniques. However, it does rely on relatively high temperatures (e.g. 0.75 T_M, where T_M is the absolute melting temperature of the substrate material) and applied pressure to achieve the reaction kinetics that would allow for relatively rapid bonding to occur [37]. Even with these excessive bonding temperatures and applied pressures, the times required to create strong, homogeneous diffusion bonds can be extreme.

To compliment the problems of high bonding temperatures and times, another key issue to consider when attempting to make a direct diffusion couple between two substrates is the geometry of the mating or bonding surfaces. Because this process does not involve any liquid-phase forming constituents, the two bonding surfaces must contact each other on a near atomic scale [39]. Porosity along the bond line could be the result of a lack of intimate contact between the two substrates. There are other factors which also limit the use of diffusion bonding such as the presence of oxide layers on the faying surfaces producing detrimental effects on the bond and the formation of brittle intermetallic phases forming in the diffusion zone causing poor mechanical properties [37, 40]. Also, residual stresses can be generated due to mismatches in linear expansion coefficients between the two substrate materials [40].

2.3.2 Brazing

Brazing is a widely used method of joining dissimilar materials. It can be defined simply as connecting two or more metallic materials by melting the brazing alloy whose melting temperature is significantly lower than the substrate materials [41]. Some advantages of the brazing technique are low cost simple technology, low thermal exposures, low mechanical stresses, and the ability, as a capillary joining process, to join complex geometries [37,42]. However, selection of a proper braze material is difficult due to the fact that it must satisfy several requirements including: low braze temperature, low erosion of substrate material, good wettability of substrate material, and high diffusivity and solubility with the substrate material [37,43].

The most significant difficulty with the brazing process is that the chemical composition of the bond-line is greatly different from that of the substrate material [37]. This leads to the melting temperature of bond-line remaining lower than that of the substrate material and therefore severely limits the operational temperature of the entire joint. Also, intermetallics can form at the bond-line resulting in degraded physical properties of the joint.

2.3.3 Transient Liquid Phase (TLP) Bonding

TLP bonding is hybrid process joining the brazing and diffusion bonding techniques [37,44-47]. Just like brazing, TLP bonding involves the placement of a thin metal interlayer between the two surfaces to be bonded and heating it to a temperature that is above the melting point of the interlayer but below the melting point of the substrate materials. The joint is then held at this temperature until it solidifies

isothermally due to the melting point suppressants diffusing away from the interlayer into the substrate materials [44,48]. The bonding actually occurs in six nominal steps: 1) Initial Condition 2) Dissolution of the Interlayer 3) Isothermal Solidification 4) Completion of Isothermal Solidification 5) Solid-State Homogenization 6) Final Condition [37]. These distinct steps are identified in Figure 6 [37].

Some advantages of TLP bonding include [37]:

- Ability to join complicated geometries.
- The formation of brittle intermetallic phases can be avoided and the microstructure of the bond region can resemble the bulk.
- The TLP process is isothermal. Therefore, it is an ideal joining technique for materials that are susceptible to hot cracking.
- Only requires minimal surface preparation unlike diffusion bonding.

Some disadvantages of TLP bonding are [37]:

- To avoid significant diffusion of interlayer or substrate constituents during heating which can lead to premature isothermal solidification before the joint cavity has been filled by capillary action, rapid heating may be required.
- Requires heating of the entire joint, unless an induction heating method is employed, which can lead to microstructural changes in the bulk material.
- Post bond heat treatments (PBHT) are often required to complete the chemical and microstructural homogenization processes.

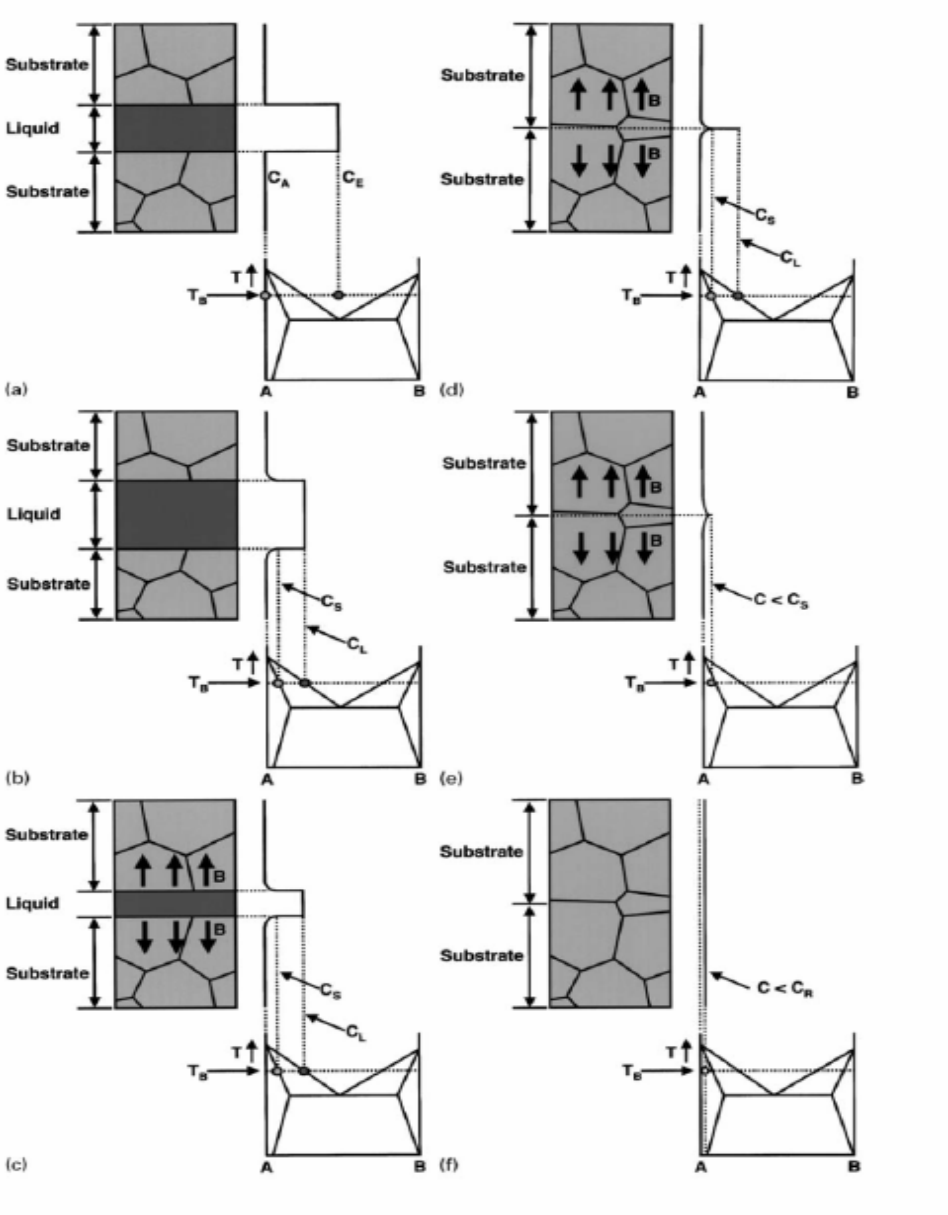

Figure 6. Stages in a TLP bonding process using a substrate with composition A (C_A) and an interlayer with eutectic composition (C_E). (a) Initial condition; (b) Dissolution of interlayer; (c) Isothermal solidification; (d) Completion of isothermal solidification; (e) Solid state homogenization; (f) Final condition; C_L = liquidus composition; C_S = solidus composition; T_B = bonding temperature [37].

3. REASEARCH OBJECTIVES

The dissimilar metal joint to be created in this work will endure excessive temperatures for long periods of time, given the fact that it will be used in a high temperature power generation system that is designed to operate at much higher efficiencies than current power generation systems. This creates the need for a joining method that will allow for the interdiffusion of the substrate species during the service life of the joint. With this situation in mind, the primary concern for the overall design of the joint is to avoid the formation of brittle intermetallic phases that could prove fatal to the system. The Ni-Nb equilibrium binary phase diagram is included as Figure 7 [49]. The intermetallic phases shown in this diagram as Ni_8Nb, Ni_3Nb, and Ni_6Nb_7 must be avoided if the joint will sustain the high temperatures and extended operational lifetimes.

In order to avoid these brittle intermetallic phases, a direct coupling of nickel to niobium must be avoided. For this reason, the two substrate metals must be kept separate from each other using an interlayer as a spacer which provides physical separation of the two substrates. Ideally these would also act as a true diffusion barrier, but the necessary diffusion data to make a suitable selection was not found in the literature. Furthermore, most candidate diffusion barriers would not produce desirable mechanical properties.

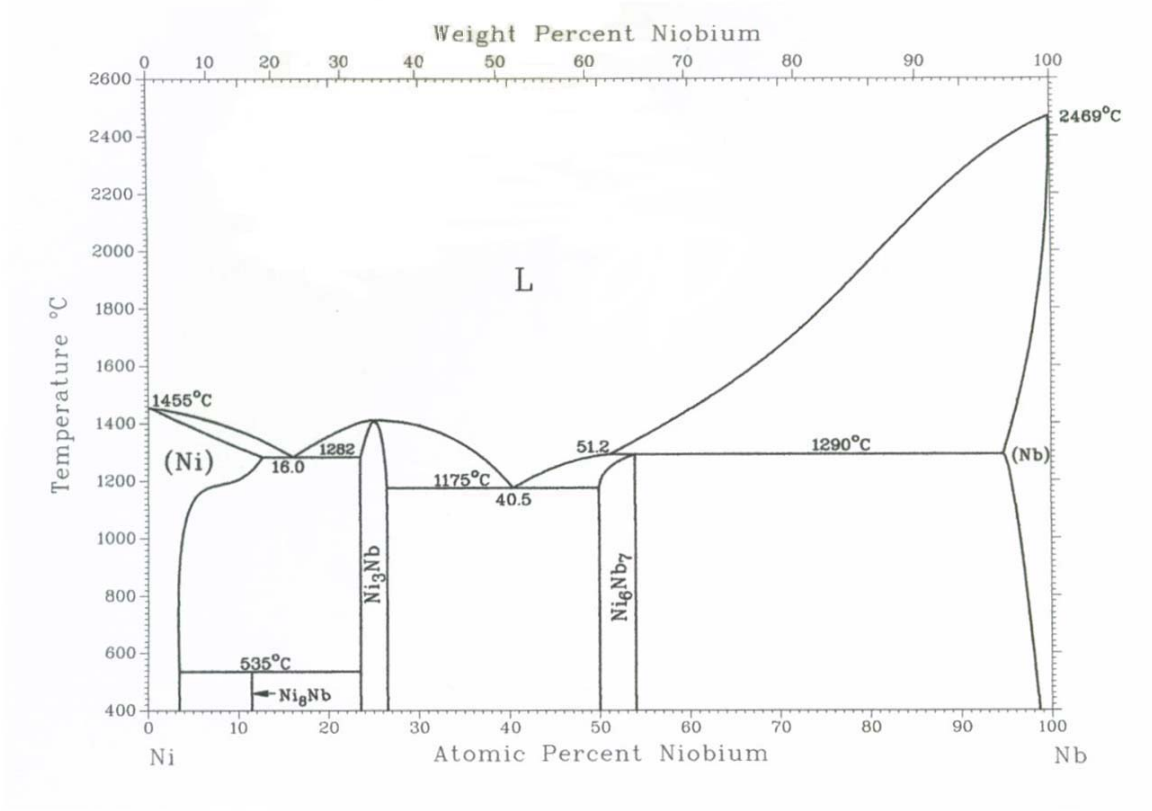

Figure 7. Ni-Nb equilibrium binary phase diagram [49].

The work documented in this thesis was completed in order to successfully create a joint between Ni and Nb substrates that would allow for long-term, high temperature operation of a high efficiency power generation system.

4. JOINT MATERIALS AND EXPERIMENTAL PROCEDURES

4.1 Possible Joint Combinations

Due to the fact that a direct coupling of Ni and Nb is impossible given that intermetallics will form and can be detrimental to the mechanical properties of the bond, spacer interlayers were used to provide a physical separation of the two substrates. In practice, no single interlayer was found to be suitable and it was necessary to employ several metallic interlayers. These interlayers are intended to be a permanent feature of the bonds, in contrast to the transient liquid phase (TLP) interlayers discussed in this chapter. To avoid confusion, the two types of interlayers will henceforth be referred to as spacer interlayers and TLP interlayers respectively.

For the initial bond design, several metallic spacer interlayers were chosen based on their respective equilibrium binary phase diagrams with the substrate materials. A comparison of all of the available system phase diagrams was completed. The primary goal of these comparisons was to select spacer interlayers that had perfect solubility with the substrate materials, so as to avoid the undesired formation of intermetallics. Comparison charts for possible combinations are included as Tables 4 through 8.

Table 5: Comparison of all available couple combinations with Ni. (*Note: The group classifications Ia-V in Tables 4 through 8 are not intended to indicate the location of these elements in the periodic table.)

Possible Ni-X Couple Combinations		
Group Classification *	Basis	Elements
Ia (Initial trials)	Solid-solution formers (at likely service temperatures)	Ir, Pd, Pt, Rh
Ib (Initial trials)	Non-intermetallic eutectic or peritectic formers (at likely service temperatures)	Cr, Os, Re, Ru, Tc
II (Secondary trials)	Intermetallic formers but with high solubility in the Ni-X system	Fe, Mo
III (Very Complex)	Forms complex intermetallic compounds with Ni or has relatively low solubility	Ta
IV (Sigma Group)	Forms undesirable σ or χ phases	V
V (Eliminated)	Various physical reasons. All of these have a binary diagram with Ni in the literature.	Ag, As, Au, B, Be, Bi, C, Ca, Cd, Ce, Co, Cu, Dy, Er, Eu, Ga, Gd, Ge, H, Hf, Hg, Ho, In, La, Mg, Mn, Nb, Nd, O, P, Pb, Po, Pr, Pu, S, Sb, Sc, Se, Si, Sm, Sn, Sr, Te, Th, Tl, Ti, Tl, U, W, Y, Yb, Zn, Zr

Table 6: Comparison of all available couple combinations with Nb. (*Note: The group classifications Ia-V in Tables 4 through 8 are not intended to indicate the location of these elements in the periodic table.)

Possible Nb-X Couple Combinations		
Group Classification *	Basis	Elements
Ia (Initial trials)	Solid-solution formers (at likely service temperatures)	Mo, Ta, Ti, V, W, Zr
Ib (Initial trials)	Non-intermetallic eutectic or peritectic formers (at likely service temperatures)	Hf
II (Secondary trials)	Intermetallic formers but with high solubility in the Nb-X system	Cr, Pd, Ru
III (Very Complex)	Forms complex intermetallic compounds with Nb or has relatively low solubility	Co, Fe, Ga, Mn, Pt
IV (Sigma Group)	Forms difficult σ or χ phases	Ir, Os, Re, Rh
V (Eliminated)	Various physical reasons. All of these have a binary diagram with Nb in the literature.	Au, B, Be, Bi, Ce, Cs, Cu, Eu, Ge, Hg, In, K, La, Mg, Na, Ni , O, Pu, Rb, S, Sb, Sc, Se, Si, Sm, Sn, Te, Th, Tl, U, Y, Yb

Table 7: Comparison of all available couple combinations with Pd. (*Note: The group classifications Ia-V in Tables 4 through 8 are not intended to indicate the location of these elements in the periodic table.)

Possible Pd-X Couple Combinations		
Group Classification *	Basis	Elements
Ia (Initial trials)	Solid-solution formers (at likely service temperatures)	Co, Fe, Ni, Pt, Rh
Ib (Initial trials)	Non-intermetallic eutectic or peritectic formers (at likely service temperatures)	Ir, Os, Re, Ru, Tc, W
II (Secondary trials)	Intermetallic formers but with high solubility in the Pd-X system	Mo, Nb, V
III (Very Complex)	Forms complex intermetallic compounds with Pd or has relatively low solubility	Be, Cr, Ta
IV (Sigma Group)	Forms difficult σ or χ phases	
V (Eliminated)	Various physical reasons. All of these have a binary diagram with Pd.	Ag, As, Au, B, Ba, Bi, C, Ca, Cd, Ce, Cu, Dy, Er, Eu, Ga, Gd, Ge, H, Hf, Hg, Ho, In, Mg, Mn, Na, Nd, P, Pb, Pr, Pu, S, Sb, Sc, Se, Si, Sm, Sn, Tb, Te, Th, Ti, Tl, U, Y, Yb, Zn, Zr

Table 8: Comparison of all available couple combinations with Pt. (*Note: The group classifications Ia-V in Tables 4 through 8 are not intended to indicate the location of these elements in the periodic table.)

Possible Pt-X Couple Combinations		
Group Classification *	Basis	Elements
Ia (Initial trials)	Solid-solution formers (at likely service temperatures)	Ir, Ni, Pd, Rh
Ib (Initial trials)	Non-intermetallic eutectic or peritectic formers (at likely service temperatures)	Os, Re, Ru, Tc, W
II (Secondary trials)	Intermetallic formers but with high solubility in the Pt-X system	Co, Cr, Fe, V
III (Very Complex)	Forms complex intermetallic compounds with Pt or has relatively low solubility	Mo, Nb, Ti
IV (Sigma Group)	Forms difficult σ or χ phases	Ta
V (Eliminated)	Various physical reasons. All of these have a binary diagram with Pt.	Ac, Ag, Am, As, Au, B, Ba, Be, Bi, C, Ca, Cd, Ce, Cm, Cu, Dy, Er, Eu, Ga, Gd, Ge, Hg, Ho, In, La, Lu, Mn, Na, Nd, P, Pb, Pr, Pu, S, Sb, Sc, Si, Sm, Sn, Sr, Tb, Te, Th, Tl, Tm, U, Y, Yb, Zn, Zr

Table 9: Comparison of all available couple combinations with Mo. (*Note: The group classifications Ia-V in Tables 4 through 8 are not intended to indicate the location of these elements in the periodic table.)

Possible Mo-X Couple Combinations		
Group Classification *	Basis	Elements
Ia (Initial trials)	Solid-solution formers (at likely service temperatures)	Cr, Nb, Ta, Ti, V, W
Ib (Initial trials)	Non-intermetallic eutectic or peritectic formers (at likely service temperatures)	Lr, Pa
II (Secondary trials)	Intermetallic formers but with high solubility in the Mo-X system	Ni, Pd, Rh
III (Very Complex)	Forms complex intermetallic compounds with Mo or has relatively low solubility	Ac, B, Ga, Hf, Lu, Pt, Th
IV (Sigma Group)	Forms difficult σ or χ phases	Co, Fe, Ir, Mn, Os, Re, Ru, Tc
V (Eliminated)	Various physical reasons. All of these have a binary diagram with Mo.	Ag, Am, As, At, Au, Ba, Be, Bi, Bk, Br, C, Ca, Cd, Ce, Cf, Cm, Cs, Cu, Dy, Er, Es, Eu, F, Fm, Fr, Gd, Ge, H, Hg, Ho, I, In, K, La, Md, Mg, Na, Nd, Ne, No, Np, O, P, Pb, Pm, Pr, Pu, Ra, Rb, S, Sb, Sc, Se, Si, Sm, Sn, Sr, Tb, Te, Tl, Tm, U, Y, Yb, Zn, Zr

Only materials from the **Ia** sections of Tables 4 through 8, with the exception of Pd being joined with Mo, were selected for bonding attempts due to perfect or near-perfect solubility with it's respective adjoining material. The Pd was chosen as a spacer interlayer because of its perfect solubility with Pt and Ni. With respect to Mo, Pd was placed in Group II because there are some intermetallics formed but given the limited operational temperature based on the Ni-based superalloy of 1000 ºC to 1100 ºC, these intermetallics are not likely to cause significant problems over the lifetime of the joint. The equilibrium binary phase diagram for the Mo-Pd system is given as Figure 8 [49]. All other materials from other sections (i.e. **Ib** through **V**) were not used in any bonding attempts for reasons as listed in the Figures.

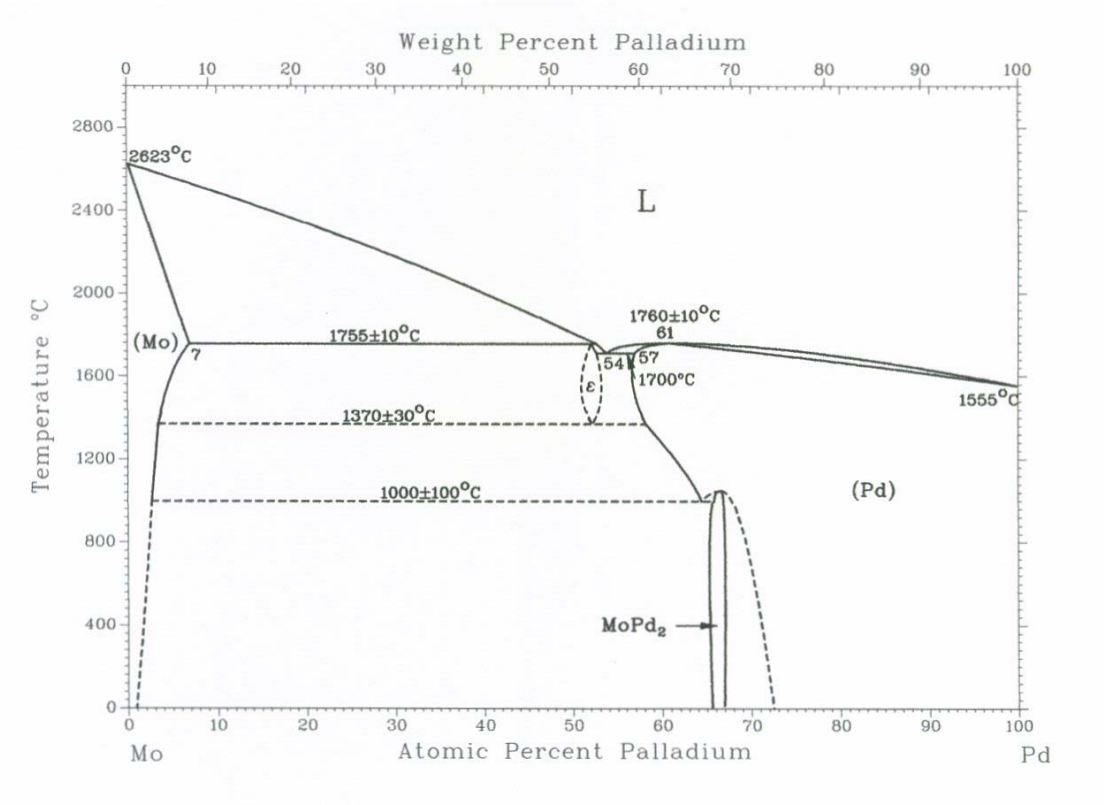

Figure 8. Mo-Pd equilibrium binary phase diagram [49].

4.2 Bonding Specimen Preparation

Substrate and spacer interlayer specimens for both the diffusion and TLP bonding attempts were prepared in the same manner. The rectangular samples were sectioned using a Struers Accutom-5 high speed wafering saw while the circular samples, used in TLP bonding, were sectioned in an electrical wire discharge machine (EDM). They were then polished in successive steps starting with 240 grit SiC paper down to 1000 grit SiC paper. This provided each specimen with smooth, flat surfaces for bonding purposes. They were then ultrasonically cleaned in an acetone bath for 15 minutes.

4.3 Diffusion Bond Design and Attempts

Based on the comparisons in Tables 4 through 8, two possible combinations of substrates and spacer interlayers were chosen for attempts at creating a diffusion couple. First, platinum was chosen as the metal to be coupled with nickel, palladium with platinum, molybdenum with palladium, and niobium with molybdenum based on perfect solubility at each of the coupled interfaces. The second possible joint combination was also attempted without platinum as the metal to be coupled with nickel. For this joint, a direct couple of nickel to palladium was attempted. Figures 9a and 9b are schematics of the diffusion couples that were attempted.

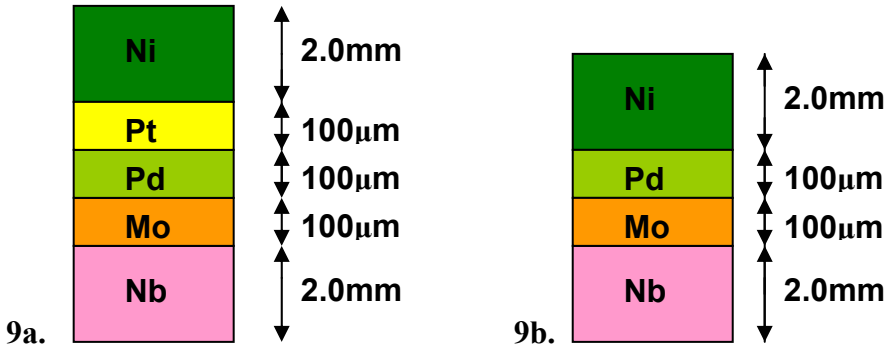

Figures 9a and 9b. Schematic of the two diffusion couples attempted. These attempts did not include any TLP interlayers.

The two stacks of metals were placed in a vacuum furnace operating at approximately 10^{-5} Pa with a tungsten weight of 1.36kg placed on top of them to maintain physical contact. The dimensions of the smallest substrate were 11.75mm x 23mm. This resulted in a net pressure of 49 kPa being placed on the stacks.

Diffusion couples with these configurations were examined for several times including 8 hours, 24 hours, 100 hours, and 200 hours at 1027ºC or 1300K. No evidence was found of undesirable behavior (e.g. formation of second phases due to diffusion right through the spacers). However, it should be cautioned that the times involved were short in comparison to the service life of the desired product. Bonding was never witnessed in either of the stacks which is desirable from a microstructural stability standpoint (but does imply that sintering alone would not serve as a bonding process). Diffusion bonding with a significant applied load was not investigated, as the final joint design is far from certain at this time and hence maximum geometrical flexibility is desired. Therefore, transient liquid phase (TLP) bonding is favored over diffusion bonding, at least at present for the intended application.

4.4 Joint Design Incorporating TLP Bonding

A new bonding scheme was developed following the failure of the diffusion bond attempts to join the spacer interlayers that involved the use of several narrow gap transient liquid phase (TLP) bonds. TLP bonding was selected for a combination of high-temperature capability and geometrical flexibility. Figure 10 is a schematic of the current bonding sequence.

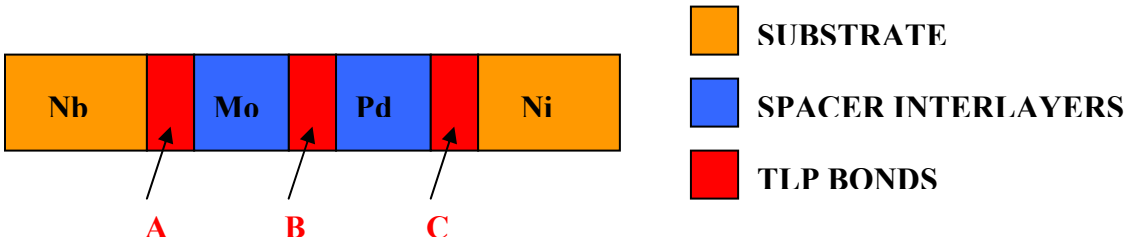

BOND	MATERIAL & PROCESSING	CURRENT STATUS
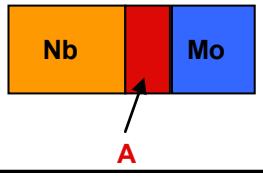	A= 25μm Ti Foil T=1850 C, t=5 hours PBHT T = 2000 C, t=4 hours	Bonds Created and Tested
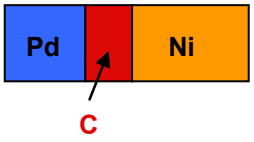	C= 25μm Ni-P (BNi-6) T=1000 C, t=3 hours	
	C= 25μm Ni-Si-B (BNi-3) T=1100 C, t=3 hours	
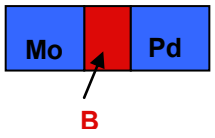	B= 80μm 76 wt.%Pd, 24 wt.%Cu Foil T=1400 C, t=1 hour in Argon atmosphere	

Figure 10. Schematic of the current bonding sequence using three distinct TLP bonds to create the overall Ni to Nb joint.

The Nb-Ti Foil-Mo, Pd-BNi3-Ni, and Pd-BNi6-Ni bonds were completed in a vacuum furnace operating at approximately 10^{-5} Pa for the times and temperatures specified in Figure 10. The nominal compositions and melting temperatures of the BNi-3 and BNi-6 TLP interlayers are given in Table 9 [50]. The Cu-Pd interlayer used in the Mo-Pd bond had to be made in an arc-melter and then rolled using a rolling mill as it was not commercially available. The interlayer composition of 76 wt.% Pd and 24 wt.% Cu was based on the systems equilibrium binary phase diagram given as Figure 11 [49] and then verified using energy-dispersive x-ray spectroscopy (EDS). The composition was selected to achieve a melting temperature of approximately 1355ºC. The bonding temperature was then set at 1400ºC.

Due to the relatively high vapor pressure of Pd (1.33 Pa at 1552ºC [51]), it was discovered experimentally that the bond could not be completed in a typical vacuum furnace. This was because, at the high gas flow rates observed in a diffusion or turbo vacuum system, Pd vapor would be removed rapidly and hence new vapor needs to be produced continuously to maintain the equilibrium vapor pressure above the Pd-bearing interlayer, leading to rapid loss of the Pd. It was decided instead to complete the bond in a tube furnace with a very low flow rate of Ar to prevent the Pd from vaporizing completely (by requiring less Pd vapor to be produced to maintain the equilibrium vapor pressure above the substrate/interlayer given the much lower gas flow rate than in a vacuum system) and losing Pd both the interlayer and substrate Pd materials.

Table 10. Nominal compositions and melting temperatures of BNi-3 and BNi-6 [50].						
	Nominal Composition (wt. %)					
Interlayer Alloy	Si	C	B	P	Ni	Liquidus Temp (°C)
BNi-3	4.5	0.06	3.2	-	Balance	1054
BNi-6	-	0.1	-	11	Balance	921

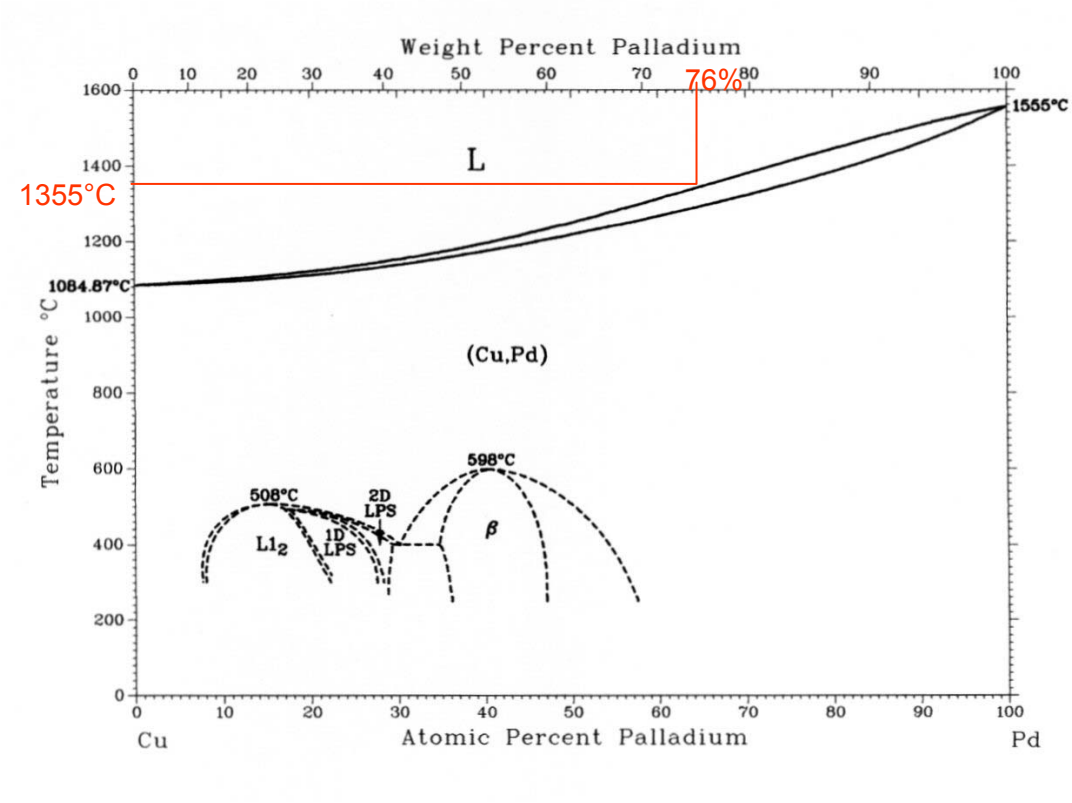

Figure 11. Cu-Pd equilibrium binary phase diagram with the TLP interlayer nominal composition annotated for the Mo-Pd bond [49].

4.5 Metallographic Sample Preparation

All of the bonded specimen samples were sectioned using a Struers Accutom-5 high speed wafering saw. After sectioning was complete, the samples were mounted for polishing using a Struers Labopress-3. Once mounted, the samples were ground to a 4000 grit SiC paper finish and then polished employing a 3μm diamond spray and 0.05μm alumina suspension solution. Three separate etchants were used on the three different bonds created. They are:

- Nb-Mo Bond: 25ml HNO_3, 5ml HF, 50ml H_2O. Immerse sample for 15-20 seconds.
- Mo-Pd Bond: 15ml HNO_3, 30ml HF, 30ml HCl. Immerse sample for 10-15 seconds.
- Pd-Ni Bond: 25ml HNO_3, 25ml HCl, 10ml H_2O. Immerse sample for 5-10 seconds.

4.6 Specimen Characterization

Characterization of all of the bonds created was completed using light microscopy. The images were enhanced using Adobe Photoshop CS with care being taken not to induce artifacts.

4.7 Mechanical Testing

The mechanical properties of each bond were studied by means of Vickers hardness tests and shear testing. The specimens used for the Vickers hardness tests were cleaned and polished via Section 4.5 but not etched.

4.7.1 Hardness Testing

Vickers microhardness testing was done on each type of bond created in order to determine the hardness diagonally across the bond-line. This provided information about the homogeneity of the microstructure in the bonded region. Microhardness testing was completed using a 300g load for a 10 second duration with traverses across the bond-line.

4.7.2 Shear Testing

Shear test specimens were sectioned using an EDM and the Struers Accutom-5 wafering saw. The dimensions used for each specimen are given in Figure 12. Three specimens for each bond were tested. Photographs of the testing apparatus are shown in Figure 13 [52].

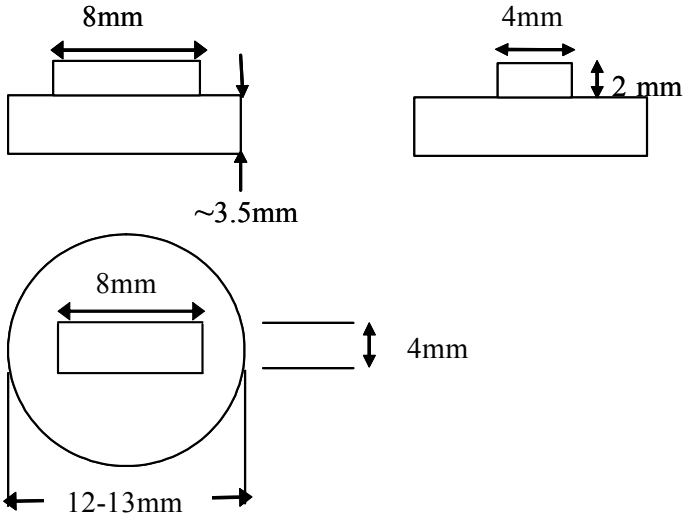

Figure 12. Diagram of shear test specimen dimensions used for each TLP bond.

Figure 13. Photographs of the shear testing device used on each TLP bond [52].

5. RESULTS AND DISCUSSION

5.1 Characterization of Individual Bonds

As mentioned in Section 4.3, bonding in the diffusion couple setup (i.e. spacer interlayers, but no TLP interlayers) was never witnessed. Therefore, only the specimens joined using the TLP procedure have been characterized. Following completion of bond formation, each bond was sectioned, polished, and chemically etched in order to characterize the observed microstructure.

5.1.1 Nb-Mo TLP Bond

The first bond created was the Nb-Mo bond using a 12.5μm Ti foil interlayer. The specimen was subjected to 1850°C for 5 hours in a vacuum furnace to produce the bond shown in Figure 14. The large black particles observed in Figure 14, as annotated, are Ti-rich and hence assumed to be α-Ti. Two heat treatments were attempted to eliminate the residual Ti; one for four hours at 2000ºC and another for eight hours at 2000ºC. Both were done in a vacuum furnace however, neither of these post bond heat treatments were successful at eliminating the α-Ti particles completely. The bond line, also annotated in the figure, displays solid contact with both the Nb and Mo substrates with very little residual Ti left. Most of the Ti has diffused into the Mo substrate.

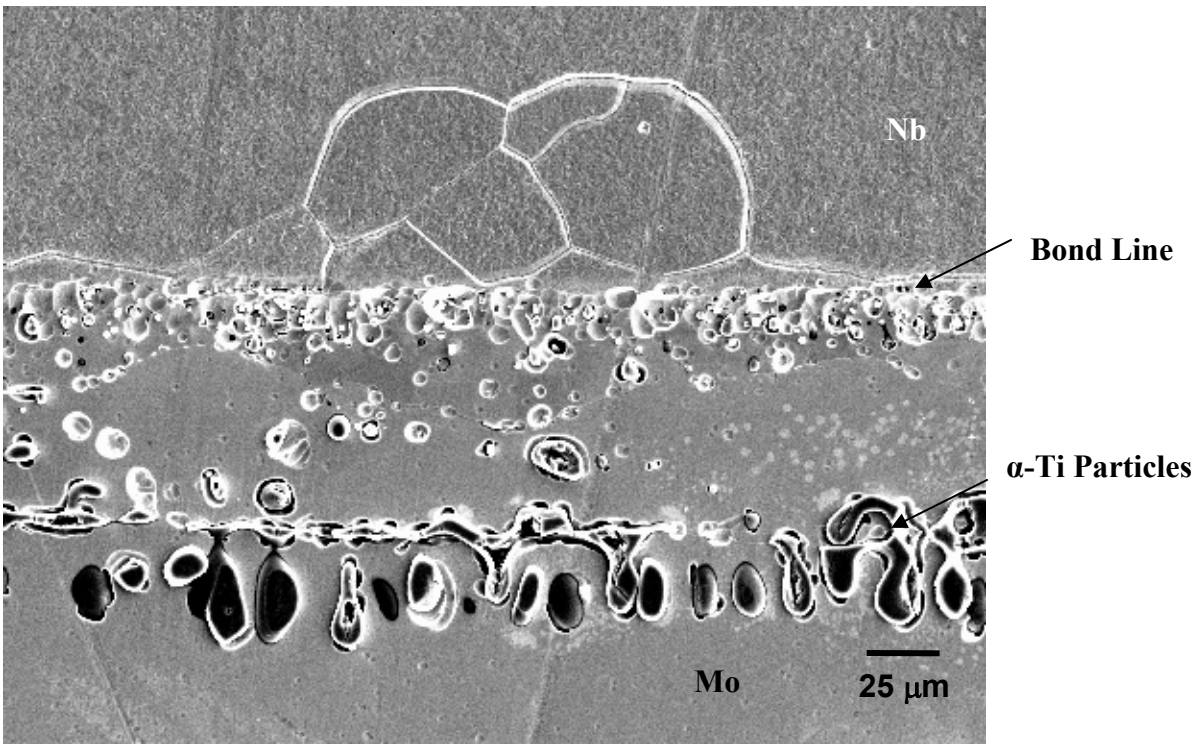

Figure 14. Micrograph of Nb-Mo TLP bond using a 12.5μm Ti interlayer.

5.1.2 Ni-Pd TLP Bonds

The Ni-Pd bond was attempted using two different TLP interlayers; BNi-6 and BNi-3. Both TLP interlayers were 25μm thick. The bond using BNi-6 completed in a vacuum furnace at 1000˚C for 3 hours while the bond incorporating BNi-3 was completed at 1100˚C for 3 hours. As seen in Figures 15 and 16, the bonds are quite similar in microstructure not withstanding expected differences in the solubility and diffusivity of P versus B in the substrates. Based on the fact that there was not enough conclusive evidence to eliminate the possibility of using either interlayer on purely microstructural grounds, both bonds were used in the testing phase to analyze and compare their respective mechanical properties.

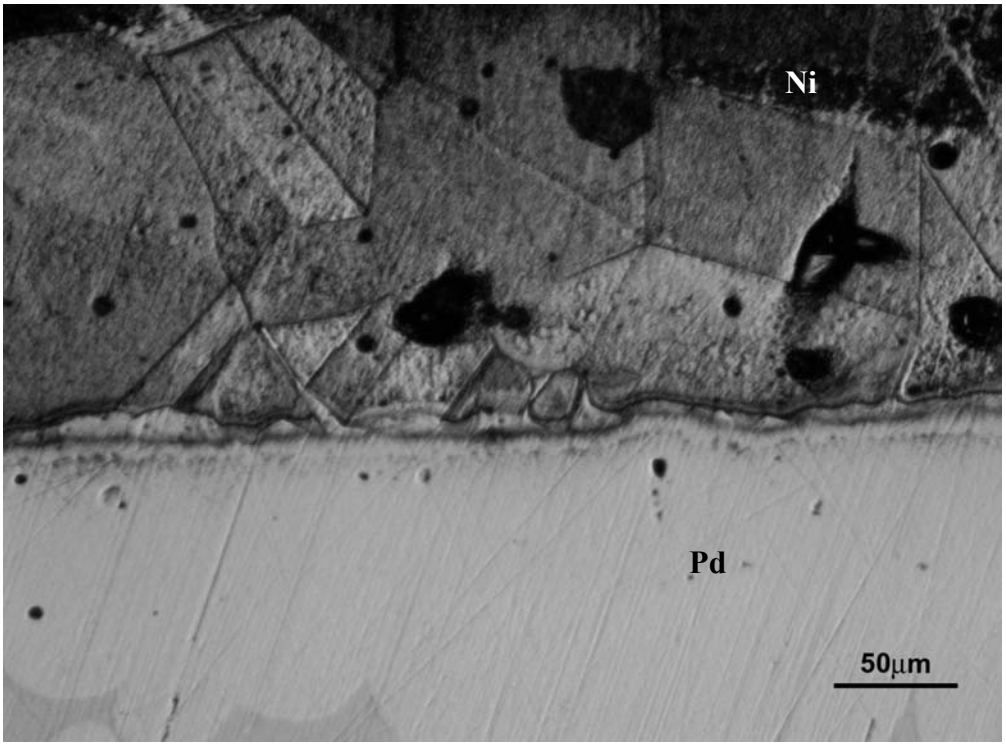

Figure 15. Micrograph of Ni-Pd TLP bond using a 25μm BNi-6 interlayer. The large dark areas in the Ni region of the bond are due to damage incurred during polishing. These might have contained phosphides, which have fallen out during polishing, although marked comet-tails were not apparent.

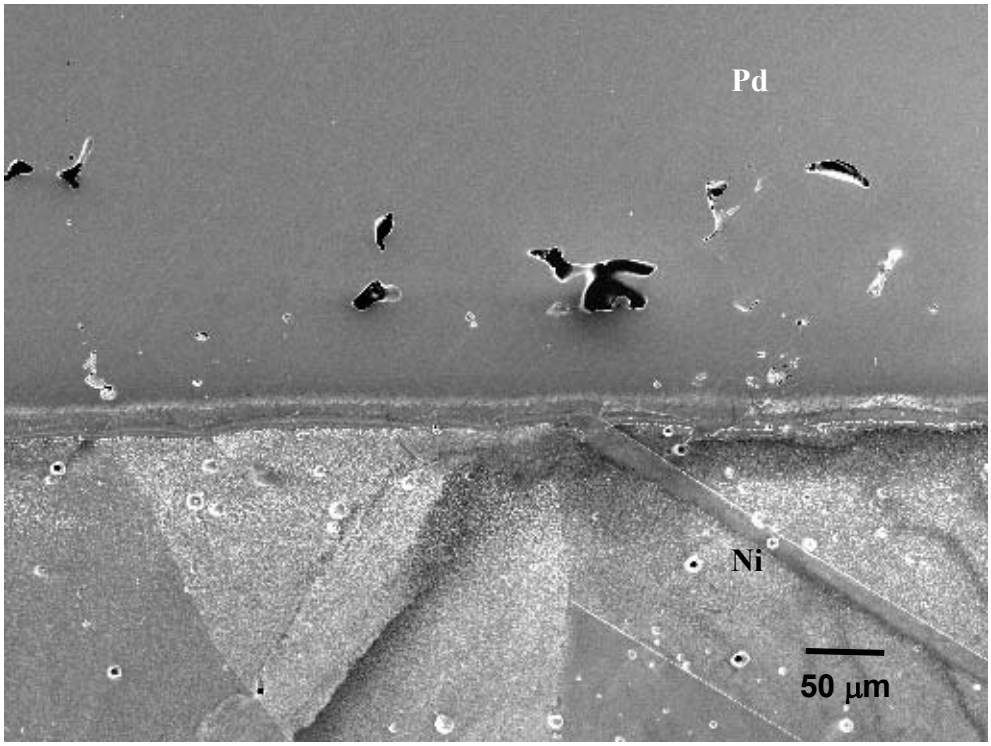

Figure 16. Micrograph of Ni-Pd TLP bond using a 25μm BNi-3 interlayer. The large dark areas in the Pd region of the bond are due to damage incurred during polishing. These might have contained borides, which have fallen out during polishing, although marked comet-tails were not apparent.

5.1.3 Mo-Pd TLP Bond

The Mo-Pd bond was the last TLP bond completed. It required the use of the TLP interlayer that was made with a composition of 76 wt.% Pd and 24 wt.% Cu as mentioned in Chapter 4.4. The final thickness of the interlayer after mechanically rolling it was 80 μm. Although the thickness of the TLP interlayer was much greater than the thickness of the TLP interlayers used in the other TLP bonds created, the bond line, as seen in Figure 17, does not display any adverse effects of using such a thick interlayer and indeed the bond represents the least marked microstructural discontinuity of all the bonds examined.

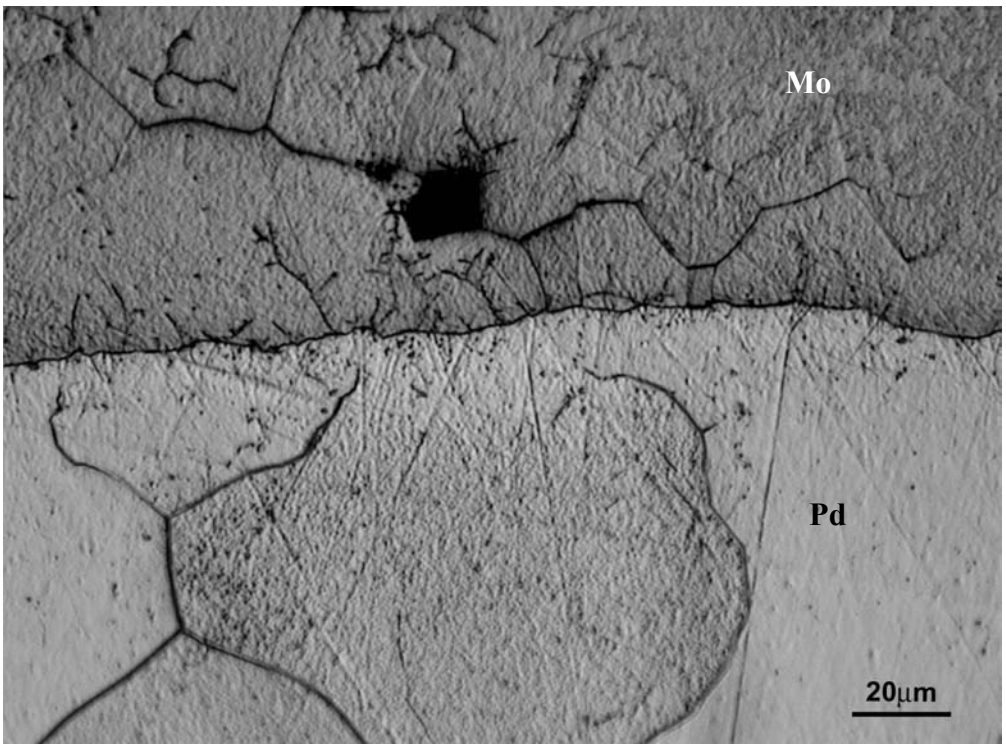

Figure 17. Micrograph of Mo-Pd TLP bond using a 0.08mm Pd-Cu interlayer. The large dark areas in the Mo region of the bond are most likely borides that fell out during polishing.

5.2 Mechanical Testing of Individual Bonds

5.2.1 Microhardness Testing

The first series of mechanical tests performed on each bond were microhardness measurements taken diagonally across each bond-line. Figures 18 and 19 are graphs of the microhardness values. Figure 19 is a graph of the relative microhardness values. There were a total of nine microhardness values taken of each bond. For relative hardness values, the average of hardness values of the first two were taken and then subtracted from the first four values. The average of hardness values of the last two were taken and then subtracted from the last four values. The average of hardness values of the first and last two were calculated then subtracted from the middle hardness value.

The graph in Figure 19 indicates there are differences in microhardness values between the bond-lines and the bulk substrate material. However, Figure 18 suggests these differences are due to the transitions between substrates.

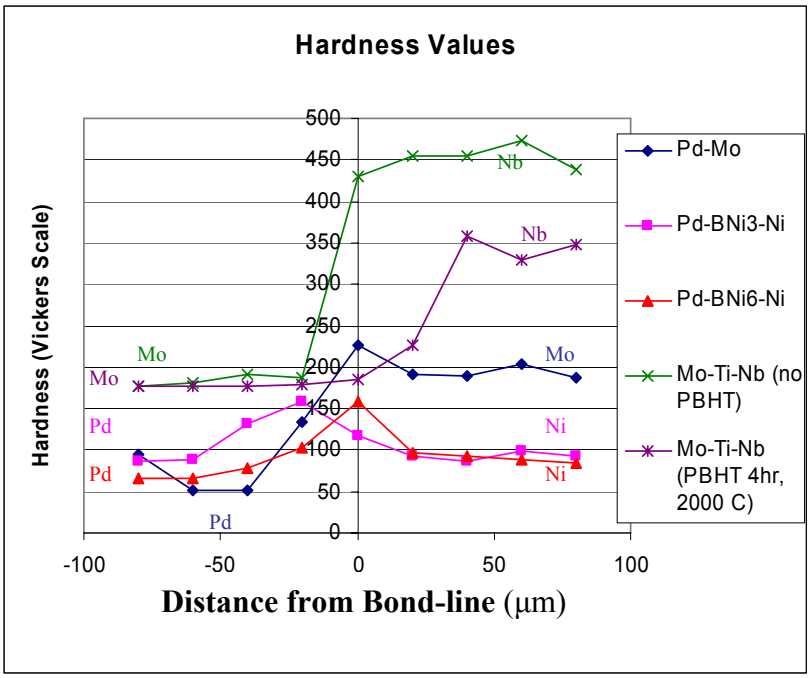

Figure 18. Graph of microhardness values taken from all TLP bonds created.

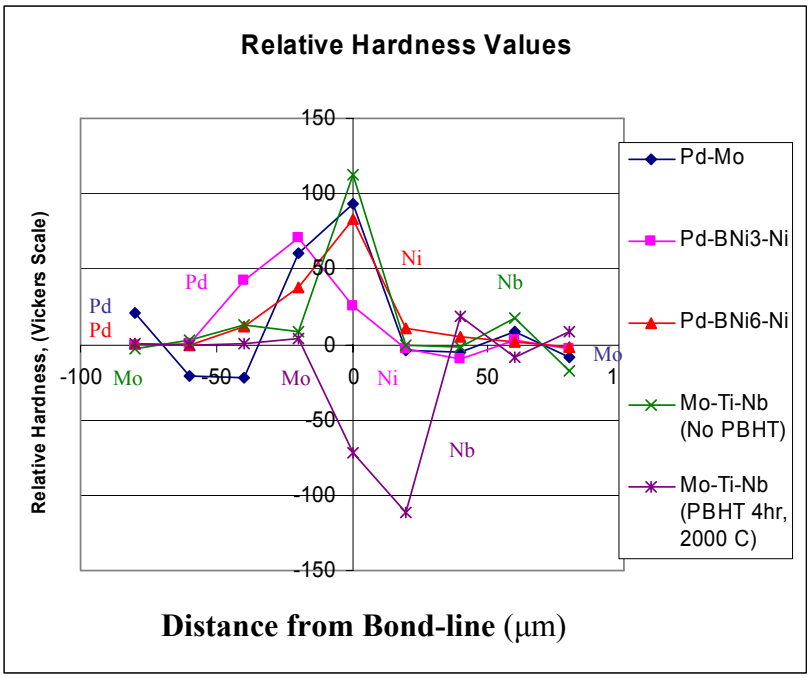

Figure 19. Graph of relative microhardness values taken from all TLP bonds created.

5.2.2 Shear Testing

Shear testing of each bond was then performed using a shear testing device shown in Figure 13 [52] from Chapter 4.7.2. Three specimens of each bond were created for the purpose of shear testing. Table 10 is a summary of the data obtained from the shear testing.

None of the bonds actually sheared in the bond-line (apart from one specimen with large non-bonded regions, apparently as a result of a fixturing failure). They all sheared in the substrate material which is indicative of strong bonding. A photograph of a Mo-Pd shear test specimen is included as Figure 20.

Table 11. Shear test data for each TLP bond used in the overall joint design. *Note, these data do not include one Mo/Ti/Nb bond specimen which had obvious non-bonded regions, due presumably to inadequate fixturing and showed a strength of only 42 MPa.

Actual Bond Shear Strengths (MPa)				
Specimen #	**Ni/BNi3/Pd**	**Ni/BNi6/Pd**	**Mo/Pd-Cu/Pd**	**Mo/Ti/Nb**
1	292.1	166	163.5	121.4
2	339.7	163.2	162.5	130.3
3	303.6	155.9	178.8	152.6
Avg.	311.8	161.7	168.27	134.77
Std. Dev.	24.84	5.21	9.14	16.07

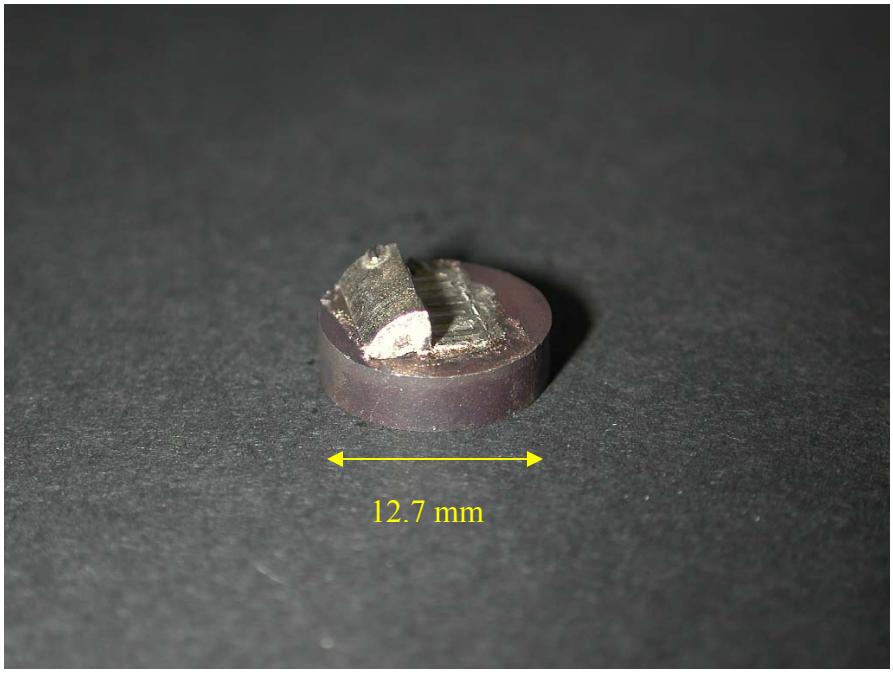

Figure 20. Photograph of Mo-Pd bond following shear testing. The upper portion if the Pd while the lower is Mo. Note that the shear failure is in the Pd, not at the bond-line.

5.3 Modeling

There are several existing models for TLP bonding [53-57]. These models tend to require complex analysis of the rate-limiting step, the isothermal solidification step [53], to calculate bond characteristics accurately. The kinetic data needed to use these models was not found in the literature. Hence, a simpler modeling method was chosen for each TLP bond that was completed. An order-of-magnitude estimation was done using Equation 1 where t was set equal to each respective bonding time along with D being the respective diffusivities for each bond. Diffusion distance (x) was then solved for to determine if the attempts at the various TLP bonds were appropriately successful.

$$x \cong \sqrt{Dt} \tag{1}$$

A few key assumptions have to be made in order to use this equation:

- The value of D is independent of concentration gradients.
- A constant temperature exists throughout the sample.
- There are no local phase transformations that would cause a change in the value of D.

The value of D was obtained either directly from the literature if it was available or it was calculated using the Arrhenius relationship in Equation 2.

$$D = A\exp(-Q/RT) \tag{2}$$

Where A is the frequency factor, Q is the activation energy, T is the temperature, and R is the gas constant equal to 8.134 kJ/mol·K. Solving these two equations provided the diffusion distances for each bond.

5.3.1 The Nb-Ti-Mo TLP Bond

The required diffusion data was readily available for both Ti in Mo and Ti in Nb. However, a key assumption had to be made concerning D_{Ti}^{Mo} = 3.19x10^{-13} m^2/s [58]. This data is for a temperature range of 1200-1400°C while the bond was created at 1850°C. Therefore, the data was extrapolated twice to 1850°C using two different values for Q commonly seen in a substitutional-type diffusion system for a refractory metal (i.e. 300 kJ/mol and 650 kJ/mol). The two values calculated for D_{Ti}^{Mo} were 3.23x10^{-13} m^2/s and 3.26x10^{-13} m^2/s. After substituting in the appropriate values and completing the calculation of Equation 1, a total diffusion distance of approximately 80 μm was obtained using both values calculated for D_{Ti}^{Mo}. This value is similar to what was actually observed as the α-Ti particles diffused approximately 100 μm into the Mo substrate. Therefore, the temperature assumption used above did not have a large negative affect on the calculation of diffusion distance.

For the diffusion of Ti in Nb, a value for D_{Ti}^{Nb} had to be calculated given A= 1.0x10^{-4} m^2/s and Q= 381 kJ/mol over a temperature range of 1973-2473 K [23]. Here an assumption has to be made due to the fact that the diffusion data is given for 89 at.% purity in the Nb. The calculated D_{Ti}^{Nb} equals 4.2x10^{-14} m^2/s at 1850°C. Overall, this results in a calculated diffusion distance of approximately 30 μm. This value is significantly less than that calculated for the Mo. Due to the uncertainty of the diffusion coefficients, the actual conditions following bond cycling are unknown. Figure 21 [59] is a diagram showing three different solute concentration lines in the bond substrates at

three different times and also a room-temperature solubility limit for α-Ti on cooling in both substrates taken from the respective binary phase diagrams.

Three possible scenarios could result depending on where in the diagram the bond was created:

- Shortest time: Small amount of α-Ti at interface.
- Middle time: α-Ti diffuses out to distance of solubility limit.
- Longest time: No α-Ti present due to Ti being less than the solubility limit.

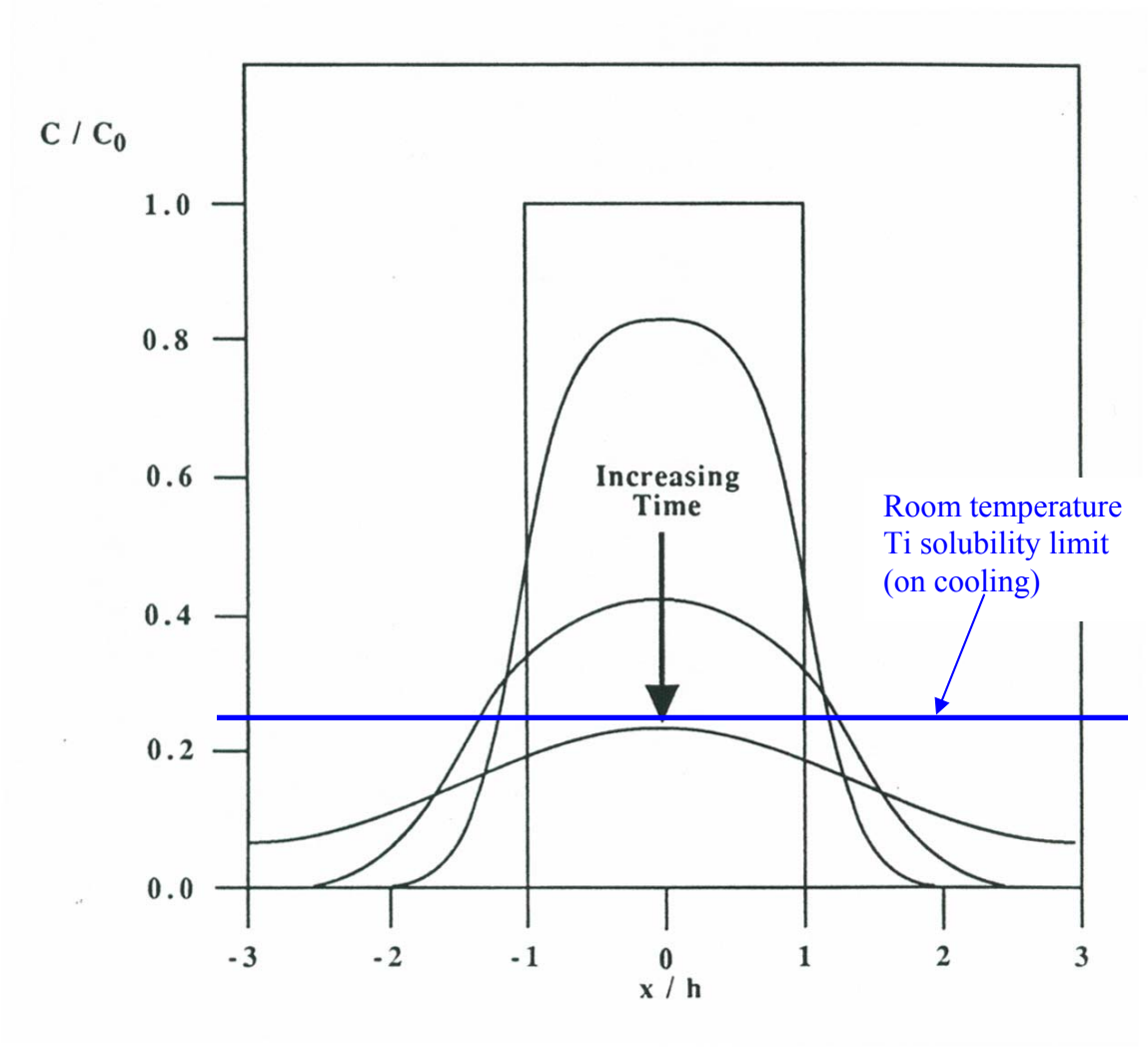

Figure 21: Three different solute concentration lines in the bond substrates at three different times and also a theoretical solubility limit for α-Ti in both substrates [59].

5.3.2 The Pd-BNi6-Ni TLP Bond

For this bond, an assumption has to be made that the primary diffusing constituent is the same constituent that serves as the melting point depressant, i.e. phosphorus (P). Diffusion data for P in Ni was not able to be located so γ-Fe was used in place of Ni. These atoms are similar in size and both metals have the same crystal structure (FCC) [60]. Therefore, the substitution should not greatly affect the outcome of the calculations due to the fact that both would experience substitutional-type of diffusion mechanisms with a similar value for Q and D expected. Therefore, D_P^{Fe} was calculated to be 7.3×10^{-14} m^2/s using the values of $A = 6.3 \times 10^{-6}$ m^2/s and Q= 193.4 kJ/mol [23]. A final value for diffusion distance was calculated to be approximately 30 μm.

For the diffusion of P into Pd, the same material (γ-Fe) is used in place of Pd due again to the similar atomic size and crystal structure [60]. Therefore, the same diffusion distance of approximately 30 μm is calculated for P into Pd. This leads to the conclusion that a uniform bond would be the result of this TLP procedure. Figure 15 displays this result with the exception of the phosphides seen in the Ni side of the bond.

5.3.3 The Pd-BNi3-Ni TLP Bond

The melting point depressant in BNi-3 is boron (B). Therefore, the calculations used for this bond are for the diffusion distance of B in both Ni and Pd. A value of 1.43×10^{-10} m^2/s for D_B^{Ni} was calculated using the quantities A= 6.6×10^{-7} m^2/s and Q= 96.3 kJ/mol [61]. The diffusion distance for B in Ni was calculated to be approximately 400 μm.

For the diffusion of the B into Pd, a stand-in had to be made for both the solvent and solute. C was used in place of B, based on their similar atomic size, and Co was used in place of Pd. Co has a similar atomic size to Pd and is also face-centered cubic (FCC) [60]. Using this data and substituting in the bond temperature of 1100ºC, a value of 4.4×10^{-11} m^2/s was calculated for D_C^{Co} using the values A= 3.1×10^{-5} m^2/s and Q= 153.7 kJ/mol [23]. Approximately 700 μm was obtained for the diffusion distance of B in this system. More borides were visible in the Pd region of the bond as shown in Figure 16. However, this could be a simple matter of the solubility of B being higher in the Ni than in the Pd and not a product of the calculated diffusion distances obtained in the modeling and given the inaccuracies of the calculations due to the numerous assumptions that were made to complete those calculations.

5.3.4 The Mo-Pd/Cu-Pd TLP Bond

The melting point depressant in the TLP interlayer for this system is Cu. Therefore, the modeling was done based on equations for the diffusion of Cu in both the Mo and Pd substrates. Data was not found for diffusion of Cu in Pd, however, data was

found for the diffusion of Cu in Pt. Pt and Pd are very similar in atomic size and structure [60] and therefore, an assumption is made that Cu will behave similarly in Pt as it will in Pd. Another assumption has to be made concerning the temperature at which the bond was created and the temperature range over which the data is valid for according to the literature. The data has a useful range of 1098-1375ºC while the bond was completed at 1400ºC and therefore the assumption is that the diffusion of Cu in Pd will behave similarly both at 1375ºC and 1400ºC. There will be a lower amount of discrepancy in this assumption than the assumption made concerning temperature in the diffusion of Ti in Mo from Section 5.3.1 due to the fact that D_{Cu}^{Pt} was calculated from A and Q. Therefore, bonding temperature was taken into account. A value of 1.24×10^{-13} m^2/s was calculated for D_{Cu}^{Pt} using the quantities A= 7.4×10^{-6} m^2/s and Q= 59.5 kJ/mol [62]. This value for Q seems quite low for a substitutional-type diffusion system. However, in the source of the data, no specific information was given concerning the method of obtaining the value. The resultant diffusion distance for Cu in Pd using the calculated diffusion constant is approximately 20 μm.

Two more assumptions had to be made for calculating the diffusion distance of Cu in Mo. The first is that diffusion data could not be found for Cu in Mo, however, data was located for substitutional diffusion of Ni in Mo. Cu and Ni are similar in atomic size and therefore both would rely on substitutional-type diffusion into Mo. The second assumption concerns the bonding temperature (1400ºC) and the temperature for which the data was given (1350ºC) [23]. Again, it must be assumed that the Cu would behave similarly at both of these temperatures with the understanding that this is likely to cause

significant errors, just as in the case of Ti diffusion in Mo, due to the exponential dependence of D on temperature. The value for D_{Ni}^{Mo} is given as a range between 2.4-3.2x10^{-16} m^2/s [23]. The higher end of this range was chosen for this calculation as the temperature at which the bond is formed is 50°C above the temperature given for the diffusion data. Using this value, a distance of 1 μm was calculated for the diffusion distance of Cu in Mo. This value is significantly less that the value calculated for the substitutional diffusion of Cu into Pd. However, the bond, as seen in the micrograph in Figure 17, is mostly uniform with the exception of the large boride seen at about 20-25 μm from the bond-line in the Mo region. The considerable number of assumptions made to calculate the two diffusion distances for this bond led to significant errors in the results.

6. SUMMARY AND CONCLUSIONS

With nickel-based superalloys and Nb being the strongest potential candidate materials for structural applications in high temperature and high efficiency power generation systems, a suitable joining technique is needed to produce a joint that minimizes changes to the base metal properties of the substrate materials. Direct bonding of the Ni and Nb substrates is not an option given the complex binary equilibrium phase diagram of the Ni-Nb system which contains several brittle intermetallic phases. These brittle phases could prove detrimental to a high temperature power generation system.

The joint design, developed in this project, is comprised of several individual TLP bonds between a series of spacer interlayers, which act as diffusion barriers, and the substrates. All of the TLP bonds are successful in terms of initial microstructure/microhardness and room-temperature mechanical testing.

There were no significant adverse effects of any microstructural anomalies that were witnessed in the micrographs in any of the TLP bonds completed. This conclusion is drawn upon by considering both the room-temperature shear testing completed and the microhardness measurements taken diagonally across each bond-line. None of the bonds actually sheared in the bond-line (apart from one specimen with large non-bonded regions, apparently as a result of a fixturing failure). They all sheared in the substrate material which is indicative of strong bonding. In addition to this testing, microhardness

measurements taken on bonded specimens indicated differences in hardness values between the bond-lines and either of the bulk materials. However, these differences are apparently due to the transitions between substrate materials.

A simple and rough modeling attempt was made for all TLP bonds created. The calculations proved to be somewhat accurate in predicting the results of the bonding experiments with the exceptions of the Pd-BNi3-Ni and Mo-Pd/Cu-Pd bonds. The errors in these calculations were probably due to the significant number of assumptions that had to be made due to the unavailability of diffusion data for the systems employed in this work.

7. RECOMMENDATIONS FOR FUTURE WORK

- The current design is based on using the pure substrates Ni and Nb. Further experimentation and adaptation must be done to accommodate for the final alloys to be used in the actual power system design.
- All testing completed was done at room temperature. Therefore, there is no high temperature data available at this time.
- There is no long term data that would indicate joint properties for target lifetimes of a high efficiency power generation system. Accelerated aging should be done in order to gain more insight on long term characteristics.
- Another consideration of the current joint design is joint geometry. Only simple butt joints were used for experimentation and testing. The final joint geometry will have to be tested once it is designed.
- Once the final joint design and geometry is decided on, careful consideration must be placed on the coefficient of thermal expansion (CTE) for each material in the bonding sequence as significant mismatches in CTE's can lead to premature failure of the joint.
- Microstructural anomalies that were witnessed in the experimental bonds need to be identified and the mechanisms inducing these need to be studied.

- The bonds created could be used to further develop kinetic data for these specific systems.
- The final recommendation is to test the joints' thermal fatigue properties.

8. REFERENCES

1. R. Tanaka: *Mater. at High Temp.*, 2000, 14(4), pp. 457-464.

2. J.B. Marriott: *Mater. & Design,* 1990, 11(3), pp. 122-128.

3. G.W. Meetham: *Mater. & Design,* 1988, 9(4), pp. 213-219.

4. C. Barbosa, J.L. Nascimento, I.M.V. Caminha, and I.C. Abud: *Eng. Failure Analysis,* 2005, 12, pp. 348-361.

5. H.W. Chuang, D.W. Liaw, Y.C. Du, and R.K. Shiue: *Mater. Sci. Eng. A,* 2005, 390, pp. 350-361.

6. C.H. Cadden and B.C. Odegard Jr.: *J. Nuc. Mater.,* 2000, 283-287, pp. 1253-1257.

7. M.H. Scott and P.M. Knowlson: *J. Less-Common Metals,* 1963, 5, pp. 205-244.

8. W.F. Gale: *J. Mater. Sci.,* 1999, 51, pp. 49-52.

9. B. Dang: Masters thesis, Auburn University, Auburn, AL, 2000.

10. C.F. McDonald and D.G. Wilson: *Appl. Therm. Eng.,* 1996, 16(8/9), pp. 635-653.

11. V.I. Kuprianov: *Renewable and Sustainable Energy Rev.,* 2005, 9, pp. 474-498.

12. "Greenhouse Gases, Climate Change, and Energy." Greenhouse Gases Programs. 2004. Energy Information Administration. Accessed on 12 Oct 2005. <http://www.eia.doe.gov/oiaf/1605/ggccebro/chapter1.html>.

13. T.H. Kwon: *Ecological Economics*, 2005, 53, pp. 261-275.

14. M. Manera and A. Marzullo: *Environmental Modelling & Software*, 2005, 20, pp. 1389-1400.

15. R. Bowman. "Superalloys: A Primer and History." 2000. Accessed on 24 Oct 2005. <http://www.tms.org/Meetings/Specialty/Superalloys2000/SuperalloysHistory.html>.

16. M.J. Donachie and S.J. Donachie: *Superalloys: a technical guide*, 2 nd ed., AMS International, Materials Park, OH, 2002.

17. M.J. Pomeroy: *Mater. & Design,* 2005, 26, pp. 223-231.

18. M. Konter and M. Thumann: *J. Mater. Process. Tech.,* 2001, 117, pp. 386-390.

19. T.E. Reed-Hill and R. Abbaschian: *Physical Metallurgy Principles*, 3rd Edition, PWS Publishing Company, Boston, MA**,** 1994**.**

20. M. Tacikowski, J.Sloma, M. Wozniak, and T. Wierzchon: *Intermetallics,* 2005, 14, pp. 123-129.

21. J. Zhou and J.T. Guo: *Mater. Sci. Eng. A,* 2003, 339, pp. 166-174.

22. Y. Mishima, E.H. Lee, and C.T. Liu: *Mater. Trans.,* 1995, 36(8), pp. 1031-1040.

23. W. F. Gale and T. C. Totemeier (Eds.): *Smithells Metals Reference Book*, 8th Edition, Butterworth-Heinemann, Oxford, 2004.

24. C.L. Ma, J.G. Li, Y. Tan, R. Tanaka, and S. Hanada: *Mater. Sci. and Eng. A,* 2004, 386, pp. 375-383.

25. Z. Zhao, L Zhang, J. Zheng, H. Bai, S. Zhang, and B. Xu: *Scripta Mater.,* 2005, 53, pp. 995-1000.

26. Q. Huang and L. Zhu: *Mater. Lett.,* 2005, 59, pp. 1732-1735.

27. S.T. Mileiko: *Composites Sci. and Tech.,* 2005, 65, pp. 2500-2513.

28. M.F. Zawrah and M.H. Aly: *Ceram. Int.,* 2005, 32, pp. 21-28.

29. M. Rosso: *J. Mater. Process. Tech., 2005 (in press).*

30. L.S. Aboyon, H.H. Nesisyan, S.L. Kharatyan, R. Orru, R. Saiu, G. Cao, and D. Zedda: *Ceram. Int.,* 2001, 27, pp. 163-169.

31. E.R. Olivas, J.G. Swadener, and Y.-L. Shen: *Scripta Mater.*, 2005, 54, pp. 263-268.

32. P. Cavaliere: *Composites: Part A,* 2005, 36, pp. 1657-1665.

33. ASM International Handbook Committee: *Heat-Resistant Materials*, 1st Edition, ASM International, Materials Park, OH, 1997.

34. M.S. El-Genk and J. Tournier: *J. Nuc. Mater.,* 2005, 340, pp. 93-112.

35. I. Hong and C. Koo: *Mater. Chem. and Phys.*, 2005, 94, pp. 131-140.

36. C.B. Geller, R.W. Smith, J.E. Hack, P. Saxe, and E. Wimmer: *Scripta Mater.,* 2005, 52, pp. 205-210.

37. D.A. Butts: PhD thesis, Auburn University, Auburn, AL, 2005.

38. W. Juan, L. Yajiang, and M. Haijun: *Vacuum,* 2005, 79, pp. 45-51.

39. M.G. Nicholas: *Joining Process.: Introduction to Brazing and Diffusion Bonding,* Klower Academic Publishers, Boston, MA, 1998.

40. S. Kundu, M. Ghosh, A. Laik, K. Bhanumurthy, G.B. Kale, and S. Chatterjee: *Mater. Sci. and Eng. A,* 2005, 407, pp. 154-160.

41. M. Uzkut, N.S. Koksal, and B.S. Unlu: *J. Mater. Process. Tech.,* 2005, 169, pp. 409-413.

42. X. Zhou, G. Qu, J. Zhou, and X. Wang: *J. Mater. Process. Tech.,* 2005, 168, pp. 280-285.

43. H. Kestler and H. Clemens: *"Production, Processing and Application of Gamma (TiAl) Based Alloys," in Titanium and Titanium Alloys,* ed. C. Leyens and M. Peters, Wiley-VCH, Germany, 2003.

44. G. Humpston and D.M. Jacobson: *ASM Int.,* 1996, pp. 128-129.

45. R.K. Saha, S. Wei, and T.I. Khan: *Mater. Sci. and Eng. A,* 2005, 406, pp. 319-327.

46. O.A. Idowu, N.L. Richards, and M.C. Chaturvedi: *Mater. Sci. and Eng. A,* 2005, 397, pp. 98-112.

47. W.F. Gale, D.A. Butts, M.Di Ruscio, and T. Zhou: *Metall. and Mater. Trans. A,* 2002, 33A, pp. 3205-3214.

48. T. Padron, T.I. Khan, and M.J. Kabir: *Mater. Sci. and Eng. A,* 2004, 385, pp. 220-228.

49. Binary Alloy Phase Diagrams, 2nd Edition, Version 1.0, ASM International Software, Materials Park, OH, 1996.

50. "Metglas Brazing – Material Specifications / Classifications." Metglas. 2004. Metglas Inc. Accessed on 17 Nov 2005. <http://www.metglas.com/products/page5_1_1_2_1.htm>.

51. "Periodic Information Part 2." Stillwater Palladium. 2004. Accessed on 17 Nov 2005. <http://stillwaterpalladium.com/periodic2.html>.

52. P. Yan and E.R. Wallach: *Intermetallics*, 1993, 1, pp. 83-97.

53. W. Tillman and E. Lugscheider: *Int. J. for the Joining of Materials*, 1996, 8(2), pp. 56-61.

54. Y. Zhou, W. F. Gale, and T. H. North: *International Materials Reviews*, 1995, 40(5), pp. 181-196.

55. O. A. Ojo, N. L. Richards, and M. C. Chaturvedi: *Science and Technology of Welding and Joining*, 2004, 9(6), pp. 532-540.

56. W. F. Gale and D. A. Butts: *Science and Technology of Welding and Joining*, 2004, 9(4), pp. 283-300.

57. T. Padron, T. I. Khan, and M. J. Kabir: *Mater. Sci. and Eng. A,* 2004, 385, pp. 220-228.

58. K. Majima and T. Isomoto: *J. Jpn. Soc. Powder Metall.*, 1982, 29(8), pp. 280-285.

59. W. F. Gale: PhD thesis, University of Cambridge, Cambridge, UK, 1991.

60. B.D. Cullity and S. R. Stock: *Elements of X-Ray Diffraction*, 3rd Edition, Prentice Hall, Upper Saddle River, NJ, 2001.

61. R. B. McLellan: *Scripta Metallurgica et Materialia*, 1995, 8, pp. 1265-1267.

62. R. Weast, M. Astle, and W. Beyer (Eds.): *CRC Handbook of Chemistry and Physics*, 66th Edition, CRC Press, Inc., Boca Raton, FL, 1986.